

1 **Estimates of Late Cenozoic climate change relevant to Earth**

2 **surface processes in tectonically active orogens**

3

4 Sebastian G. Mutz¹, Todd A. Ehlers¹, Martin Werner², Gerrit Lohmann², Christian Stepanek²,
5 Jingmin Li^{1,3}

6 ¹Department of Geosciences, University Tübingen, D-72074 Tübingen, Germany

²Department of Paleoclimate Dynamics, Alfred Wegener Institute, Helmholtz Centre for Polar and Marine Research, D-
27570 Bremerhaven, Germany

³now at Institute for Geography and Geology, University of Würzburg, Würzburg, D-97074 Germany

7

8 *Correspondence to:* Sebastian G. Mutz (sebastian.mutz@uni-tuebingen.de)

9

10 **Abstract**

11 The denudation history of active orogens is often interpreted in the context of modern climate gradients. Here we
12 address the validity of this approach and ask the question: what are the spatial and temporal variations in palaeoclimate
13 for a latitudinally diverse range of active orogens? We do this using high-resolution (T159, ca. 80 x 80 km at the
14 equator) palaeoclimate simulations from the ECHAM5 global Atmospheric General Circulation Model and a statistical
15 cluster analysis of climate over different orogens (Andes, Himalaya, SE Alaska, Pacific NW USA). Time periods and
16 boundary conditions considered include the Pliocene (PLIO, ~3 Ma), the Last Glacial Maximum (LGM, ~21 ka), Mid
17 Holocene (MH, ~6 ka) and Pre-Industrial (PI, reference year 1850). The regional simulated climates of each orogen are
18 described by means of cluster analyses based on the variability of precipitation, 2m air temperature, the intra-annual
19 amplitude of these values, and monsoonal wind speeds where appropriate. Results indicate the largest differences to the
20 PI climate existed for the LGM and PLIO climates in the form of widespread cooling and reduced precipitation in the
21 LGM and warming and enhanced precipitation during the PLIO. The LGM climate shows the largest deviation in
22 annual precipitation from the PI climate, and shows enhanced precipitation in the temperate Andes, and coastal regions
23 for both SE Alaska and the US Pacific Northwest. Furthermore, LGM precipitation is reduced in the western
24 Himalayas and enhanced in the eastern Himalayas, resulting in a shift of the wettest regional climates eastward along
25 the orogen. The cluster-analysis results also suggest more climatic variability across latitudes east of the Andes in the
26 PLIO climate than in other time-slice experiments conducted here. Taken together, these results highlight significant
27 changes in Late Cenozoic regional climatology over the last ~3 Ma. Comparison of simulated climate with proxy-based
28 reconstructions for the MH and LGM reveal satisfactory to good performance of the model in reproducing precipitation
29 changes, although in some cases discrepancies between neighbouring proxy observations highlight contradictions
30 between proxy observations themselves. Finally, we document regions where the largest magnitudes of Late Cenozoic

31 changes in precipitation and temperature occur and offer the highest potential for future observational studies that
32 quantify the impact of climate change on denudation and weathering rates.

33

34 **Keywords:** Cenozoic climate, ECHAM5, Last Glacial Maximum, Mid-Holocene, Pliocene, cluster analysis, Himalaya,
35 Tibet, Andes, Alaska, Cascadia

36

37 **1. Introduction**

38 Interpretation of orogen denudation histories in the context of climate and tectonic interactions is often hampered
39 by a paucity of terrestrial palaeoclimate proxy data needed to reconstruct spatial variations in palaeoclimate. While it is
40 self-evident that palaeoclimate changes could influence palaeodenudation rates, it is not always self-evident what the
41 magnitude of climate change over different geologic time scales is, or what geographic locations offer the greatest
42 potential to investigate palaeoclimate impacts on denudation. Palaeoclimate reconstructions are particularly beneficial
43 when denudation rates are determined using geo- and thermo-chronology techniques that integrate over timescales of
44 10^3 - 10^6 years (e.g. cosmogenic radionuclides or low-temperature thermochronology) [e.g., Kirchner et al., 2001;
45 Schaller et al., 2002; Bookhagen et al., 2005; Moon et al., 2011; Thiede and Ehlers, 2013; Lease and Ehlers, 2013].
46 However, few studies using denudation rate determination methods that integrate over longer timescales have access to
47 information about past climate conditions that could influence these palaeo-denudation rates. Palaeoclimate modelling
48 offers an alternative approach to sparsely available proxy data for understanding the spatial and temporal variations in
49 precipitation and temperature in response to changes in orography [e.g. Takahashi and Battisti, 2007a, b; Insel et al.,
50 2010; Feng et al., 2013] and global climate change events [e.g. Salzman, 2011; Jeffery et al., 2013]. In this study, we
51 characterise the climate at different times in the Late Cenozoic, and the magnitude of climate change for a range of
52 active orogens. Our emphasis is on identifying changes in climate parameters relevant to weathering and catchment
53 denudation to illustrate the potential importance of various global climate change events on surface processes.

54 Previous studies of orogen-scale climate change provide insight into how different tectonic or global climate
55 change events influence regional climate change. For example, sensitivity experiments demonstrated significant
56 changes in regional and global climate in response to landmass distribution and topography of the Andes, including
57 changes in moisture transport, the north-south asymmetry of the Intertropical Convergence Zone [e.g. Takahashi and
58 Battisti, 2007a, ; Insel et al., 2010] and (tropical) precipitation [Maroon et al., 2015, ; 2016]. Another example is the
59 regional and global climate changes induced by the Tibetan Plateau surface uplift due to its role as a physical obstacle to
60 circulation [Raymo and Ruddiman, 1992; Kutzbach et al., 1993; Thomas, 1997; Bohner, 2006; Molnar et al., 2010;
61 Boos and Kuang, 2010]. The role of tectonic uplift in long term regional and global climate change remains a focus of

62 research and continues to be assessed with geologic datasets [e.g. Dettman et al., 2003; Caves et al., 2017; Kent-
63 Corson et al., 2006; Lechler et al., 2013; Lechler and Niemi, 2011; Licht et al., 2016; Methner et al.,
64 2016; Mulch et al., 2015, 2008; Pingel et al., 2016] and climate modelling [e.g. Kutzbach et al., 1989; Kutzbach
65 et al., 1993; Zhisheng, 2001; Bohner, 2006; Takahashi and Battisti, 2007a; Ehlers and Poulsen, 2009; Insel et al., 2010;
66 Boos and Kuang, 2010]. Conversely, climate influences tectonic processes through erosion [e.g. Molnar and England,
67 1990; Whipple et al., 1999; Montgomery et al., 2001; Willett et al., 2006; Whipple, 2009]. Quaternary climate change
68 between glacial and interglacial conditions [e.g. Braconnot et al., 2007; Harrison et al., 2013] resulted in not only the
69 growth and decay of glaciers and glacial erosion [e.g. Yanites and Ehlers, 2012; Herman et al., 2013; Valla et al., 2011]
70 but also global changes in precipitation and temperature [e.g. Otto-Bliesner et al., 2006; Li et al., 2017] that could
71 influence catchment denudation in non-glaciated environments [e.g. Schaller and Ehlers, 2006; Glotzbach et al., 2013;
72 Marshall et al., 2015]. These dynamics highlight the importance of investigating how much climate has changed over
73 orogens that are the focus of studies of climate-tectonic interactions and their impact on erosion.

74 Despite recognition by previous studies that climate change events relevant to orogen denudation are prevalent
75 throughout the Late Cenozoic, few studies have critically evaluated how different climate change events may, or may
76 not, have affected the orogen climatology, weathering and erosion. Furthermore, recent controversy exists concerning
77 the spatial and temporal scales over which geologic and geochemical observations can record climate-driven changes in
78 weathering and erosion [e.g. Whipple, 2009; von Blanckenburg et al., 2015; Braun, 2016]. For example, the previous
79 studies highlight that although palaeoclimate impacts on denudation rates are evident in some regions and measurable
80 with some approaches, they are not always present (or detectable) and the spatial and temporal scale of climate change
81 influences our ability to record climate sensitive denudation histories. This study contributes to our understanding of
82 the interactions between climate, weathering, and erosion by bridging the gap between the palaeoclimatology and
83 surface processes communities by documenting the magnitude and distribution of climate change over tectonically
84 active orogens.

85 Motivated by the need to better understand climate impacts on Earth surface processes, especially the denudation
86 of orogens, we model palaeoclimate for four time slices in the Late Cenozoic, use descriptive statistics to identify the
87 extent of different regional climates, quantify changes in temperature and precipitation, and discuss the potential
88 impacts on fluvial and/or hillslope erosion. In this study, we employ the ECHAM5 global Atmospheric General
89 Circulation Model and document climate and climate change for time slices ranging between the Pliocene (PLIO, ~3
90 Ma) to pre-industrial (PI) times for the St. Elias Range of South East Alaska, the US Pacific Northwest (Olympic and
91 Cascade Range), western South America (Andes) and South Asia (incl. parts of Central- and East Asia). Our approach is
92 two-fold and includes:

93 1. An empirical characterisation of palaeo-climates in these regions based on the covariance and spatial

94 clustering of monthly precipitation and temperature, the monthly change in precipitation and temperature magnitude,
95 and wind speeds where appropriate.

96 2. Identification of changes in annual mean precipitation and temperature in selected regions for four time
97 periods: (PLIO, Last Glacial Maximum (LGM), the Mid-Holocene (MH) and PI) and subsequent validation of the
98 simulated precipitation changes for MH and LGM.

99 Our focus is on documenting climate and climate change in different locations with the intent of informing past and
100 ongoing palaeodenudation studies of these regions. The results presented here also provide a means for future work to
101 formulate testable hypotheses and investigations into whether or not regions of large palaeoclimate change produced a
102 measurable signal in denudation rates or other Earth surface processes. More specifically, different aspects of the
103 simulated palaeoclimate may be used as boundary conditions for vegetation and landscape evolution models, such as
104 LPJ-GUESS and Landlab, to bridge the gap between climate change and quantitative estimates for Earth surface system
105 responses. In this study, we intentionally refrain from applying predicted palaeoclimate changes to predict denudation
106 rate changes. Such a prediction is beyond the scope of this study because a convincing (and meaningful) calculation of
107 climate-driven transients in fluvial erosion (e.g. via the kinematic wave equation), variations in frost cracking intensity,
108 or changes in hillslope sediment production and transport at the large regional scales considered here is not tractable
109 within a single manuscript, and instead is the focus of our ongoing work. Merited discussion of climatically induced
110 changes in glacial erosion, as is important in the Cenozoic, is also beyond the scope of this study. Instead, our emphasis
111 lies on providing and describing a consistently setup GCM simulation framework for future investigations of Earth
112 surface processes, and to identify regions in which Late Cenozoic climate changes potentially have a significant impact
113 on fluvial and hillslope erosion.

114

115 **2. Methods: Climate modelling and cluster analyses for climate characterisation**

116

117 **2.1 ECHAM5 simulations**

118 The global Atmospheric General Circulation Model ECHAM5 [Roeckner et al., 2003] has been developed at the
119 Max Planck Institute for Meteorology and is based on the spectral weather forecast model of the ECMWF [Simmons et
120 al., 1989]. In the context of palaeoclimate applications, the model has been used mostly at lower resolution (T31, ca.
121 3.75°x3.75°; T63, ca. 1.9°x1.9° in case of Feng et al. [2016] and T106 in the case of Li et al. [2016] and Feng and
122 Poulsen [2016]). The performed studies are not limited to the last millenium [e.g. Jungclaus et al., 2010] but also
123 include research in the field of both warmer and colder climates, at orbital [e.g. Gong et al., 2013; Lohmann et al., 2013;
124 Pfeiffer and Lohmann, 2016; Zhang et al., 2013a; Zhang et al., 2014; Wei and Lohmann, 2012] and tectonic time scales
125 [e.g. Knorr et al., 2011; Stepanek and Lohmann, 2012], and under anthropogenic influence [Gierz et al., 2015].

126 Here, the ECHAM5 simulations were conducted at a T159 spatial resolution (horizontal grid size ca. 80 km x 80
127 km at the equator) with 31 vertical levels (between the surface and 10hPa). This high model resolution is admittedly not
128 required for all of the climatological questions investigated in this study, and it should be noted that the skill of GCM's
129 in predicting orographic precipitation remains limited at this scale [e.g. Meehl et al. 2007]. However, simulations were
130 conducted at this resolution so that future work can apply the results in combination with different dynamical and
131 statistical downscaling methods to quantify changes at large catchment to orogen scales. The output frequency is
132 relatively high (1 day) to enhance the usefulness of our simulations as input for landscape evolution and other models
133 that may benefit from daily input. The simulations were conducted for five different time periods: present-day (PD), PI,
134 MH, LGM and PLIO.

135 A PD simulation (not shown here) was used to establish confidence in the model performance before conducting
136 palaeosimulations and has been compared with the following observation-based datasets: European Centre for Medium-
137 Range Weather Forecasts (ECMWF) re-analyses [ERA40, Uppala et al., 2005], National Centers for Environmental
138 Prediction and National Center for Atmospheric Research (NCEP/NCAR) re-analyses [Kalnay et al., 1996; Kistler et
139 al., 2001], NCEP Regional Reanalysis (NARR) [Mesinger et al., 2006], the Climate Research Unit (CRU) TS3.21
140 dataset [Harris et al., 2013], High Asia Refined Analysis (HAR30) [Maussion et al., 2014] and the University of
141 Delaware dataset (UDEL v3.01) [Legates et al., 1990]. (See Mutz et al. [2016] for a detailed comparison with a lower
142 resolution model).

143 The PI climate simulation is an ECHAM5 experiment with PI (reference year 1850) boundary conditions. Sea
144 Surface Temperatures (SST) and Sea Ice Concentration (SIC) are derived from transient coupled ocean-atmosphere
145 simulations [Lorenz and Lohmann, 2004; Dietrich et al., 2013]. Following Dietrich et al. [2013], greenhouse gas
146 (GHG) concentrations (CO₂: 280 ppm) are taken from ice core based reconstructions of CO₂ [Etheridge et al., 1996],
147 CH₄ [Etheridge et al., 1998] and N₂O [Sowers et al., 2003]. Sea surface boundary conditions for MH originate from a
148 transient, low-resolution, coupled atmosphere-ocean simulation of the mid (6 ka) Holocene [Wei and Lohmann, 2012;
149 Lohmann et al, 2013], where the GHG concentrations (CO₂: 280 ppm) are taken from ice core reconstructions of
150 GHG's by Etheridge et al. [1996], Etheridge et al. [1998] and Sowers et al. [2003]. GHG's concentrations for the LGM
151 (CO₂: 185 ppm) have been prescribed following Otto-Bliesner et al. [2006]. Orbital parameters for MH and LGM are
152 set according to Dietrich et al. [2013] and Otto-Bliesner et al. [2006], respectively. LGM land-sea distribution and ice
153 sheet extent and thickness are set based on the PMIP III (Palaeoclimate Modelling Intercomparison Project, phase 3)
154 guidelines (elaborated on by Abe-Ouchi et al [2015]). Following Schäfer-Neth and Paul [2003], SST and SIC for the
155 LGM are based on GLAMAP [Sarnthein et al. 2003] and CLIMAP [CLIMAP project members, 1981] reconstructions
156 for the Atlantic and Pacific/Indian Ocean, respectively. Global MH and LGM vegetation are based on maps of plant
157 functional types by the BIOME 6000 / Palaeovegetation Mapping Project [Prentice et al., 2000; Harrison et al., 2001;

158 Bigelow et al., 2003; Pickett et al., 2004] and model predictions by Arnold et al. [2009]. Boundary conditions for the
159 PLIO simulation, including GHG concentrations (CO₂: 405), orbital parameters and surface conditions (SST, SIC, sea
160 land mask, topography and ice cover) are taken from the PRISM (Pliocene Research, Interpretation and Synoptic
161 Mapping) project [Haywood et al., 2010; Sohl et al., 2009; Dowsett et al., 2010], specifically PRISM3D. The PLIO
162 vegetation boundary condition was created by converting the PRISM vegetation reconstruction to the JSBACH plant
163 functional types as described by Stepanek and Lohmann [2012], but the built-in land surface scheme was used

164 SST reconstructions can be used as an interface between oceans and atmosphere [e.g. Li et al. 2016] instead of
165 conducting the computationally more expensive fully coupled Atmosphere-Ocean GCM experiments. While the use of
166 SST climatologies comes at the cost of capturing decadal-scale variability, and the results are ultimately biased towards
167 the SST reconstructions the model is forced with, the simulated climate more quickly reaches an equilibrium state and
168 the means of atmospheric variables used in this study do not change significantly after the relatively short spin-up
169 period. The palaeoclimate simulations (PI, MH, LGM, PLIO) using ECHAM5 are therefore carried out for 17 model
170 years, of which the first two years are used for model spin up. The monthly long-term averages (multi-year means for
171 individual months) for precipitation, temperature, as well as precipitation and temperature amplitude, i.e. the mean
172 difference between the hottest and coldest months, have been calculated from the following 15 model years for the
173 analysis presented below.

174 For further comparison between the simulations, the investigated regions were subdivided (Fig. 1). Western
175 South America was subdivided into four regions: parts of tropical South America (80°-60° W, 23.5°-5° S), temperate
176 South America (80°-60° W, 50°-23.5° S), tropical Andes (80°-60° W, 23.5°-5° S; high-pass filtered), i.e. most of the
177 Peruvian Andes, Bolivian Andes and northernmost Chilean Andes, and temperate Andes (80°-60° W, 50°-23.5° S, high-
178 pass filtered). South Asia was subdivided into three regions: tropical South Asia (40°-120°E, 0°-23.5°N), temperate
179 South Asia (40°-120°E, 23.5°-60°N), and high altitude South Asia (40°-120°E, 0°-60°N; high-pass filtered).

180 Our approach of using a single GCM (ECHAM5) for our analysis is motivated by, and differs from, previous
181 studies where inter-model variability exists from the use of different GCMs due to different parameterisations in each
182 model. The variability in previous inter-model GCM comparisons exists despite the use of the same forcings [e.g. see
183 results highlighted in IPCC AR5]. Similarities identified between these palaeoclimate simulations conducted with
184 different GCMs using similar boundary conditions can establish confidence in the models when in agreement with
185 proxy reconstructions. However, differences identified in inter-model GCM comparisons highlight biases by all or
186 specific GCMs, or reveal sensitivities to one changed parameter, such as model resolution. Given these limitations of
187 GCM modelling, we present in this study a comparison of a suite of ECHAM5 simulations to proxy-based
188 reconstructions (where possible) and, to a lesser degree, comment on general agreement or disagreement of our
189 ECHAM5 results with other modelling studies. A detailed inter-model comparison of our results with other GCMs is

190 beyond the scope of this study, and better suited for a different study in a journal with a different focus and audience.
191 Rather, by using the same GCM and identical resolution for the time slice experiments, we reduce the number of
192 parameters (or model parameterisations) varying between simulations and thereby remove potential sources of error or
193 uncertainty that would otherwise have to be considered when comparing output from different models with different
194 parameterisations of processes, model resolution, and in some cases model forcings (boundary conditions).
195 Nevertheless, the reader is advised to use these model results with the GCM's shortcoming and uncertainties in
196 boundary condition reconstructions in mind. For example, precipitation results may require dynamical or statistical
197 downscaling to increase accuracy where higher resolution precipitation fields are required. Furthermore, readers are
198 advised to familiarise themselves with the palaeogeography reconstruction initiatives and associated uncertainties. For
199 example, while Pliocene ice sheet volume can be estimated, big uncertainties pertaining to their locations remain
200 [Haywood et al. 2010].

201

202 **2.2 Cluster analysis to document temporal and spatial changes in climatology**

203 The aim of the clustering approach is to group climate model surface grid boxes together based on similarities in
204 climate. Cluster analyses are statistical tools that allow elements (i) to be grouped by similarities in the elements'
205 attributes. In this study, those elements are spatial units, the elements' attributes are values from different climatic
206 variables, and the measure of similarity is given by a statistical distance. The four basic variables used as climatic
207 attributes of these spatial elements are: near-surface (2m) air temperature, seasonal 2m air temperature amplitude,
208 precipitation rate, and seasonal precipitation rate amplitude. Since monsoonal winds are a dominant feature of the
209 climate in the South Asia region, near surface (10m) speeds of u-wind and v-wind (zonal and meridional wind
210 components, respectively) during the monsoon season (July) and outside the monsoon season (January) are included as
211 additional variables in our analysis of that region. Similarly, u-wind and v-wind speeds during (January) and outside
212 (July) the monsoon season in South America are added to the list of considered variables to take into account the South
213 American Monsoon System (SASM) in the cluster analysis for this region. The long-term monthly means of those
214 variables are used in a hierarchical clustering method, followed by a non-hierarchical k-means correction with
215 randomised re-groupment [Mutz et al., 2016; Wilks, 2011; Paeth, 2004; Bahrenberg et al., 1992].

216 The hierarchical part of the clustering procedure starts with as many clusters as there are elements (n_i), then
217 iteratively combines the most similar clusters to form a new cluster using centroids for the linkage procedure for
218 clusters containing multiple elements. The procedure is continued until the desired number of clusters (k) is reached.
219 One disadvantage of a pure hierarchical approach is that elements cannot be re-categorised once they are assigned to a
220 cluster, even though the addition of new elements to existing clusters changes the clusters' defining attributes and could
221 warrant a re-categorisation of elements. We address this problem by implementation of a (non-hierarchical) k-means

222 clustering correction [e.g. Paeth, 2004]. Elements are re-categorised based on the multivariate centroids determined by
223 the hierarchical cluster analysis in order to minimize the sum of deviations from the cluster centroids. The Mahalanobis
224 distance [e.g. Wilks, 2011] is used as a measure of similarity or distance between the cluster centroids, since it is a
225 statistical distance and thus not sensitive to different variable units. The Mahalanobis distance also accounts for possible
226 multi-collinearity between variables.

227 The end results of the cluster analyses are subdivisions of the climate in the investigated regions into k
228 subdomains or clusters based on multiple climate variables. The region-specific k has to be prescribed before the
229 analyses. A large k may result in redundant additional clusters describing very similar climates, thereby defeating the
230 purpose of the analysis to identify and describe the dominant, distinctly different climates in the region and their
231 geographical coverage. Since it is not possible to know a priori the ideal number of clusters, k was varied between 3 and
232 10 for each region and the results presented below identify the optimal number of visibly distinctly different clusters
233 from the analysis. Optimal k was determined by assessing the distinctiveness and similarities between the climate
234 clusters in the systematic process of increasing k from 3 to 10. Once an increase in k no longer resulted in the addition
235 of another cluster that was climatologically distinctly different from the others, and instead resulted in at least two
236 similar clusters, k of the previous iteration was chosen as the optimal k for the region.

237 The cluster analysis ultimately results in a description of the geographical extent of a climate (cluster)
238 characterised by a certain combination of mean values for each of the variables associated with the climate. For
239 example, climate cluster 1 may be the most tropical climate in a region and thus be characterised by a high precipitation
240 values, high temperature values and low seasonal temperature amplitude. Each of the results (consisting of the
241 geographical extent of climates and mean vectors describing the climate) can be viewed as an optimal classification for
242 the specific region and time. It serves primarily as a means for providing an overview of the climate in each of the
243 regions at different times, reduces dimensionality of the raw simulation output, and identify regions of climatic
244 homogeneity that is difficult to notice by viewing simple maps of each climate variable. Its synoptic purpose is similar
245 to that of the widely known Köppen-Geiger classification scheme [Peel et al., 2007], but we allow for optimal
246 classification rather than prescribe classes, and our selection of variables is more restricted and made in accordance with
247 the focus of this study.

248

249 **3. Results**

250 Results from our analysis are first presented for general changes in global temperature and precipitation for the
251 different time slices (Fig. 2, 3), which is then followed by an analysis of changes in the climatology of selected orogens.
252 A more detailed description of temperature and precipitation changes in our selected orogens is presented in subsequent
253 subsections (Fig. 4 and following). All differences in climatology are expressed relative to the PI control run. Changes

254 relative to the PI rather than PD conditions are presented to avoid interpreting an anthropogenic bias in the results and
255 focusing instead on pre-anthropogenic variations in climate. For brevity, near-surface (2m) air temperature and total
256 precipitation rate are referred to as temperature and precipitation.

257

258 **3.1 Global differences in mean annual temperature**

259 This section describes the differences between simulated MH, LGM, and PLIO annual mean temperature anom-
260 alies with respect to PI shown in Fig. 2b, and PI temperature absolute values shown in Fig. 2a. Most temperature differ-
261 ences between the PI and MH climate are within -1°C to 1°C . Exceptions to this are the Hudson Bay, Weddell Sea and
262 Ross Sea regions which experience warming of $1-3^{\circ}\text{C}$, $1-5^{\circ}\text{C}$ and $1-9^{\circ}\text{C}$ respectively. Continental warming is mostly re-
263 stricted to low-altitude South America, Finland, western Russia, the Arabian Peninsula ($1-3^{\circ}\text{C}$) and subtropical north
264 Africa ($1-5^{\circ}\text{C}$). Simulation results show that LGM and PLIO annual mean temperature deviate from the PI means the
265 most. The global PLIO warming and LGM cooling trends are mostly uniform in direction, but the magnitude varies re-
266 gionally. The strongest LGM cooling is concentrated in regions where the greatest change in ice extent occurs (as indic-
267 ated on Fig. 2), i.e. Canada, Greenland, the North Atlantic, Northern Europe and Antarctica. Central Alaska shows no
268 temperature changes, whereas coastal South Alaska experiences cooling of $\leq 9^{\circ}\text{C}$. Cooling in the US Pacific northwest
269 is uniform and between 11 and 13°C . Most of high-altitude South America experiences mild cooling of $1-3^{\circ}\text{C}$, $3-5^{\circ}\text{C}$ in
270 the central Andes and $\leq 9^{\circ}\text{C}$ in the south. Along the Himalayan orogen, LGM temperature values are $5-7^{\circ}\text{C}$ below PI
271 values. Much of central Asia and the Tibetan plateau cools by $3-5^{\circ}\text{C}$, and most of India, low-altitude China and south-
272 east Asia by $1-3^{\circ}\text{C}$.

273 In the PLIO climate, parts of Antarctica, Greenland and the Greenland Sea experience the greatest temperature
274 increase ($\leq 19^{\circ}\text{C}$). Most of southern Alaska warms by $1-5^{\circ}\text{C}$ and $\leq 9^{\circ}\text{C}$ near McCarthy, Alaska. The US Pacific northw-
275 est warms by $1-5^{\circ}\text{C}$. The strongest warming in South America is concentrated at the Pacific west coast and the Andes
276 ($1-9^{\circ}\text{C}$), specifically between Lima and Chiclayo, and along the Chilean-Argentinian Andes south of Bolivia ($\leq 9^{\circ}\text{C}$).
277 Parts of low-altitude South America to the immediate east of the Andes experience cooling of $1-5^{\circ}\text{C}$. The Himalayan
278 orogen warms by $3-9^{\circ}\text{C}$, whereas Myanmar, Bangladesh, Nepal, northern India and northeast Pakistan cool by $1-9^{\circ}\text{C}$.

279

280 **3.2 Global differences in mean annual precipitation**

281 Notable differences occur between simulated MH, LGM, PLIO annual mean precipitation anomalies with re-
282 spect to PI shown in Fig. 3b, and the PI precipitation absolute values shown in Fig. 3a. Of these, MH precipitation devi-
283 ates the least from PI values. The differences between MH and PI precipitation on land appear to be largest in northern
284 tropical Africa (increase ≤ 1200 mm/a) and along the Himalayan orogen (increase ≤ 2000 mm/a) and in central Indian
285 states (decrease) ≤ 500 mm. The biggest differences in western South America are precipitation increases in central Chile

286 between Santiago and Puerto Montt. The LGM climate shows the largest deviation in annual precipitation from the PI
287 climate, and precipitation on land mostly decreases. Exceptions are increases in precipitation rates in North American
288 coastal regions, especially in coastal South Alaska (≤ 2300 mm/a) and the US Pacific Northwest (≤ 1700 mm/a). Further
289 exceptions are precipitation increases in low-altitude regions immediately east of the Peruvian Andes (≤ 1800 mm/a),
290 central Bolivia (≤ 1000 mm/a), most of Chile (≤ 1000 mm/a) and northeast India (≤ 1900 mm/a). Regions of notable pre-
291 cipitation decrease are northern Brazil (≤ 1700 mm/a), southernmost Chile and Argentina (≤ 1900 mm/a), coastal south
292 Peru (≤ 700 mm/a), central India (≤ 2300 mm/a) and Nepal (≤ 1600 mm/a).

293 Most of the precipitation on land in the PLIO climate is higher than those in the PI climate. Precipitation is en-
294 hanced by ca. 100-200 mm/a in most of the Atacama desert, by ≤ 1700 mm/a south of the Himalayan orogen and by
295 ≤ 1400 mm/a in tropical South America. Precipitation significantly decreases in central Peru (≤ 2600 mm), southernmost
296 Chile (≤ 2600 mm) and from eastern Nepal to northernmost northeast India (≤ 2500 mm).

297

298 **3.3 Palaeoclimate characterisation from the cluster analysis and changes in regional climatology**

299 In addition to the above described global changes, the PLIO to PI regional climatology changes substantially in
300 the four investigated regions of: South Asia (section 3.3.1), the Andes (section 3.3.2), South Alaska (section 3.3.3) and
301 the Cascade Range (section 3.3.4). Each climate cluster defines separate distinct climate that is characterized by the
302 mean values of the different climate variables used in the analysis. The clusters are calculated by taking the arithmetic
303 means of all the values (climatic means) calculated for the grid boxes within each region. The regional climates are
304 referred to by their cluster number C_1, C_2, \dots, C_k , where k is the number of clusters specified for the region. The clusters
305 for specific palaeoclimates are mentioned in the text as $C_{i(t)}$, where i corresponds to the cluster number ($i=1, \dots, k$) and t
306 to the simulation time period ($t=PI, MH, LGM, PLIO$). The descriptions first highlight the similarities and then the
307 differences in regional climate. The cluster means of seasonal near-surface temperature amplitude and seasonal
308 precipitation amplitude are referred to as temperature and precipitation amplitude. The median, 25th percentile, 75th
309 percentile, minimum and maximum values for annual mean precipitation are referred to as $P_{md}, P_{25}, P_{75}, P_{min}$ and P_{max}
310 respectively. Likewise, the same statistics for temperature are referred to as $T_{md}, T_{25}, T_{75}, T_{min}$ and T_{max} . These are
311 presented as boxplots of climate variables in different time periods. When the character of a climate cluster is described
312 as “high”, “moderate” and “low”, the climatic attribute’s values are described relative to the value range of the specific
313 region in time, thus high PLIO precipitation rates may be higher than high LGM precipitation rates. The character is
314 presented a raster plots, to allow compact visual representation of it. The actual mean values for each variable in every
315 time-slice and region-specific cluster are included in tables in the supplementary material.

316

317 **3.3.1 Climate change and palaeoclimate characterisation in South Asia, Central- and East Asia**

318 This section describes the regional climatology of the four investigated Cenozoic time slices and how
319 precipitation and temperature changes from PLIO to PI times in tropical, temperate and high altitude regions. LGM and
320 PLIO simulations show the largest simulated temperature and precipitation deviations (Fig. 4b) from PI temperature and
321 precipitation (Fig. 4a) in the South Asia region. LGM temperatures are 1-7°C below PI temperatures and the direction
322 of deviation is uniform across the study region. PLIO temperature is mostly above PI temperatures by 1-7°C. The
323 cooling of 3-5°C in the region immediately south of the Himalayan orogen represents one of the few exceptions.
324 Deviations of MH precipitation from PI precipitation in the region are greatest along the eastern Himalayan orogeny,
325 which experiences an increase in precipitation (≤ 2000 mm/a). The same region experiences a notable decrease in
326 precipitation in the LGM simulation, which is consistent in direction with the prevailing precipitation trend on land
327 during the LGM. PLIO precipitation on land is typically higher than PI precipitation.

328 Annual means of precipitation and temperature spatially averaged for the regional subdivisions and the different
329 time slice simulations have been compared. The value range P_{25} to P_{75} of precipitation is higher for tropical South Asia
330 than for temperate and high altitude South Asia (Fig. 5 a-c). The LGM values for P_{25} , P_{md} and P_{75} are lower than for the
331 other time slice simulations, most visibly for tropical South Asia (ca. 100 mm/a). The temperature range (both $T_{75}-T_{25}$
332 and $T_{max}-T_{min}$) is smallest in the hot (ca. 21°C) tropical South Asia, wider in the high altitude (ca. -8°C) South Asia, and
333 widest in the temperate (ca. 2°C) South Asia region (Fig. 5 d-f). T_{md} , T_{25} and T_{75} values for the LGM are ca. 1°C, 1-2°C
334 and 2°C below PI and MH temperatures in tropical, temperate and high altitude South Asia respectively, whereas the
335 same temperature statistics for the PLIO simulation are ca. 1°C above PI and MH values in all regional subdivisions
336 (Fig. 5 d-f). With respect to PI and MH values, precipitation and temperature are generally lower in the LGM and higher
337 in the PLIO in tropical, temperate and high altitude South Asia.

338 In all time periods, the wettest climate cluster C_1 covers an area along the southeastern Himalayan orogen (Fig. 6
339 a-d) and is defined by the highest precipitation amplitude (dark blue, Fig. 6 e-h). $C_{5(PI)}$, $C_{3(MH)}$, $C_{4(LGM)}$ and $C_{5(PLIO)}$ are
340 characterized by (dark blue, Fig. 6e-h) the highest temperatures, u-wind and v-wind speeds during the summer monsoon
341 in their respective time periods, whereas $C_{4(PI)}$, $C_{5(MH)}$, and $C_{6(LGM)}$ are defined by low temperatures and highest
342 temperature amplitude, u-wind and v-wind speeds outside the monsoon season (in January) in their respective time
343 periods (Fig. 6 e-h). The latter 3 climate classes cover much of the more continental, northern landmass in their
344 respective time periods and represents a cooler climate affected more by seasonal temperature fluctuations (Fig. 6 a-d).
345 The two wettest climate clusters C_1 and C_2 are more restricted to the eastern end of the Himalayan orogen in the LGM
346 than during other times, indicating that the LGM precipitation distribution over the South Asia landmass is more
347 concentrated in this region than in other time slice experiments.

348
349 **3.3.2 Climate change and palaeoclimate characterisation in the Andes, Western South America**

350 This section describes the cluster analysis based regional climatology of the four investigated Late Cenozoic
351 time slices and illustrates how precipitation and temperature changes from PLIO to PI in tropical and temperate low-
352 and high altitude (i.e. Andes) regions in western South America (Fig. 7-9).

353 LGM and PLIO simulations show the largest simulated deviations (Fig. 7b) from PI temperature and
354 precipitation (Fig. 7a) in western South America. The direction of LGM temperature deviations from PI temperatures is
355 negative and uniform across the region. LGM temperatures are typically 1-3°C below PI temperatures across the region,
356 and 1-7°C below PI values in the Peruvian Andes, which also experience the strongest and most widespread increase in
357 precipitation during the LGM (≤ 1800 mm/a). Other regions, such as much of the northern Andes and tropical South
358 America, experience a decrease of precipitation in the same experiment. PLIO temperature is mostly elevated above PI
359 temperatures by 1-5°C. The Peruvian Andes experience a decrease in precipitation (≤ 2600 mm), while the northern
360 Andes are wetter in the PLIO simulation compared to the PI control simulation.

361 PI, MH, LGM and PLIO precipitation and temperature means for regional subdivisions have been compared.
362 The P_{25} to P_{75} range is smallest for the relatively dry temperate Andes and largest for tropical South America and the
363 tropical Andes (Fig. 8 a-d). P_{max} is lowest in the PLIO in all four regional subdivisions even though P_{md} , P_{25} and P_{75} in
364 the PLIO simulation are similar to the same statistics calculated for PI and MH time slices. P_{md} , P_{25} and P_{75} for the LGM
365 are ca. 50 mm/a lower in tropical South America and ca. 50 mm/a higher in the temperate Andes. Average PLIO
366 temperatures are slightly warmer and LGM temperatures are slightly colder than PI and MH temperatures in tropical
367 and temperate South America (Fig. 8 e and f). These differences are more pronounced in the Andes, however. T_{md} , T_{25}
368 and T_{75} are ca. 5°C higher in the PLIO climate than in PI and MH climates in both temperate and tropical Andes,
369 whereas the same temperatures for the LGM are ca. 2-4°C below PI and MH values (Fig. 8 g and h).

370 For the LGM, the model computes drier-than-PI conditions in tropical South America and tropical Andes,
371 enhanced precipitation in the temperate Andes, and a decrease in temperature that is most pronounced in the Andes. For
372 the PLIO, the model predicts precipitation similar to PI, but with lower precipitation maxima. PLIO temperatures
373 generally increase from PI temperatures, and this increase is most pronounced in the Andes.

374 The climate variability in the region is described by six different clusters (Fig. 9 a-d), which have similar
375 attributes in all time periods. The wettest climate C_1 is also defined by moderate to high precipitation amplitudes, low
376 temperatures and moderate to high u-wind speeds in summer and winter in all time periods (dark blue, Fig. 9 e-h). $C_{2(PI)}$,
377 $C_{2(MH)}$, $C_{3(LGM)}$ and $C_{2(PLIO)}$ are characterized by high temperatures and low seasonal temperature amplitude (dark blue,
378 Fig. 9 e-h), geographically cover the north of the investigated region, and represent a more tropical climate. $C_{5(PI)}$,
379 $C_{5(MH)}$, $C_{6(LGM)}$ and $C_{6(PLIO)}$ are defined by low precipitation and precipitation amplitude, high temperature amplitude and
380 high u-wind speeds in winter (Fig. 9 e-h), cover the low-altitude south of the investigated region (Fig. 9 a-d) and
381 represent dry, extra-tropical climates with more pronounced seasonality. In the PLIO simulation, the lower-altitude east

382 of the region has four distinct climates, whereas the analysis for the other time slice experiments only yield three
383 distinct climates for the same region.

384

385 **3.3.3 Climate change and palaeoclimate characterisation in the St. Elias Range, Southeast Alaska**

386 This section describes the changes in climate and the results from the cluster analysis for South Alaska (Fig. 10-12). As
387 is the case for the other study areas, LGM and PLIO simulations show the largest simulated deviations (Fig. 10b) from
388 PI temperature and precipitation (Fig. 10a). The sign of LGM temperature deviations from PI temperatures is negative
389 and uniform across the region. LGM temperatures are typically 1-9°C below PI temperatures, with the east of the study
390 area experiencing largest cooling. PLIO temperatures are typically 1-5°C above PI temperatures and the warming is
391 uniform for the region. In comparison to the PI simulation, LGM precipitation is lower on land, but higher (≤ 2300 mm)
392 in much of the coastal regions of South Alaska. Annual PLIO precipitation is mostly higher (≤ 800 mm) than for PI.

393 P_{md} , P_{25} , P_{75} , P_{min} and P_{max} for South Alaskan mean annual precipitation do not differ much between PI, MH and
394 PLIO climates, while P_{md} , P_{25} , P_{75} and P_{min} decrease by ca. 20-40 mm/a and P_{max} increases during the LGM (Fig. 11a).
395 The Alaskan PLIO climate is distinguished from the PI and MH climates by its higher (ca. 2°C) regional temperature
396 means, T_{25} , T_{75} and T_{md} (Fig. 11b). Mean annual temperatures, T_{25} , T_{75} , T_{min} and T_{max} are lower in the LGM than in any
397 other considered time period (Fig. 11b), and about 3-5°C lower than during the PI and MH.

398 Distinct climates are present in the PLIO to PI simulations for Southeast Alaska. Climate cluster C_1 is always
399 geographically restricted to coastal southeast Alaska (Fig. 12 a-d) and characterized by the highest precipitation,
400 precipitation amplitude, temperature, and by relatively low temperature amplitude (dark blue, Fig. 12 e-h). Climate C_2 is
401 characterized by moderate to low precipitation, precipitation amplitude, temperature, and by low temperature amplitude.
402 C_2 is either restricted to coastal southeast Alaska (in MH and LGM climates) or coastal southern Alaska (in PI and PLIO
403 climates). Climate C_3 is described by low precipitation, precipitation amplitude, temperature, and moderate temperature
404 amplitude in all simulations. It covers coastal western Alaska and separates climate C_1 and C_2 from the northern C_4
405 climate. Climate C_4 is distinguished by the highest mean temperature amplitude, by low temperature and precipitation
406 amplitude, and by lowest precipitation.

407 The geographical ranges of PI climates C_1 - C_4 and PLIO climates C_1 - C_4 are similar. $C_{1(PI/PLIO)}$ and $C_{2(PI/PLIO)}$ spread
408 over a larger area than $C_{1(MH/LGM)}$ and $C_{2(MH/LGM)}$. $C_{2(PI/PLIO)}$ are not restricted to coastal southeast Alaska, but also cover the
409 coastal southwest of Alaska. The main difference in characterization between PI and PLIO climates C_1 - C_4 lies in the
410 greater difference (towards lower values) in precipitation, precipitation amplitude and temperature from $C_{1(PLIO)}$ to
411 $C_{2(PLIO)}$ compared to the relatively moderate decrease in those means from $C_{1(PI)}$ to $C_{2(PI)}$.

412

413 **3.3.4 Climate change and palaeoclimate characterisation in the Cascade Range, US Pacific Northwest**

414 This section describes the character of regional climatology in the US Pacific Northwest and its change over time
415 (Fig. 13-15). The region experiences cooling of typically 9-11°C on land during the LGM, and warming of 1-5°C
416 during the PLIO (Fig. 13b) when compared to PI temperatures (Fig. 13a). LGM precipitation increases over water,
417 decreases on land by ≤ 800 mm/a in the North and in the vicinity of Seattle and increases on land by ≤ 1400 mm/a on
418 Vancouver Island, around Portland and the Olympic Mountains, whereas PLIO precipitation does not deviate much
419 from PI values over water and varies in the direction of deviation on land. MH temperature and precipitation deviation
420 from PI values are negligible.

421 P_{md} , P_{25} , P_{75} , P_{min} and P_{max} for the Cascade Range do not notably differ between the four time periods (Fig. 14a).
422 The LGM range of precipitation values is slightly larger than that of the PI and MH with slightly increased P_{md} , while
423 the respective range is smaller for simulation PLIO. The T_{md} , T_{25} , T_{75} and T_{max} values for the PLIO climate are ca. 2°C
424 higher than those values for PI and MH (Fig. 14b). All temperature statistics for the LGM are notably (ca. 13°C) below
425 their analogues in the other time periods (Fig. 14b).

426 PI, LGM and PLIO clusters are similar in both their geographical patterns (Fig. 15 a, c, d) and their
427 characterization by mean values (Fig. 15 e, g, h). C_1 is the wettest cluster and shows the highest amplitude in
428 precipitation. The common characteristics of the C_2 cluster are moderate to high precipitation and precipitation
429 amplitude. C_4 is characterized by the lowest precipitation and precipitation amplitudes, and the highest temperature
430 amplitudes. Regions assigned to clusters C_1 and C_2 are in proximity to the coast, whereas C_4 is geographically restricted
431 to more continental settings.

432 In the PI and LGM climates, the wettest cluster C_1 is also characterized by high temperatures (Fig 10 e, g).
433 However, virtually no grid boxes were assigned to $C_{1(LGM)}$. $C_{1(MH)}$ differs from other climate state's C_1 clusters in that it is
434 also described by moderate to high near surface temperature and temperature amplitude (Fig 10 f), and in that it is
435 geographically less restricted and, covering much of Vancouver Island and the continental coastline north of it (Fig 10
436 b). Near surface temperatures are highest for C_2 in PI, LGM and PLIO climates (Fig 10 e, g, h) and low for $C_{2(MH)}$ (Fig
437 10 f). $C_{2(MH)}$ is also geographically more restricted than C_2 clusters in PI, LGM and PLIO climates (Fig 10 a-d). $C_{2(PI)}$,
438 $C_{2(MH)}$ and $C_{2(LGM)}$ have a low temperature amplitude (Fig 10 e-g), whereas $C_{2(PLIO)}$ is characterized by a moderate
439 temperature amplitude (Fig 10 h).

440

441 4. Discussion

442 In the following, we synthesise our results and compare to previous studies that investigate the effects of
443 temperature and precipitation change on erosion. Since our results do not warrant merited discussion of subglacial
444 processes without additional work that is beyond the scope of this study, we instead advise caution in interpreting the
445 presented precipitation and temperature results in an erosional context where the regions are covered with ice. For

446 convenience, ice cover is indicated on figures 2,3,47,10 and 13, and a summary of ice cover used as boundary
447 conditions for the different time slice experiments is included in the supplemental material. Where possible, we relate
448 the magnitude of climate change predicted in each geographical study area with terrestrial proxy data.

449

450 **4.1 Synthesis of temperature changes**

451

452 **4.1.1 Temperature changes and implications for weathering and erosion**

453 Changes in temperature can affect physical weathering due to temperature-induced changes in periglacial
454 processes and promote frost cracking and frost creep [e.g., Matsuoka, 2001; Schaller et al., 2002; Matsuoka and
455 Murton, 2008; Delunel et al., 2010; Andersen et al., 2015; Marshall et al., 2015], and also biotic weathering and erosion
456 [e.g. Moulton et al., 1998; Banfield et al., 1999; Dietrich and Perron, 2006]. Quantifying and understanding past
457 changes in temperature is thus vital for our understanding of denudation histories. In the following, we highlight regions
458 in the world where future observational studies might be able to document significant warming or cooling that would
459 influence temperature related changes in physical and chemical weathering over the last ~3 Ma.

460 Simulated MH temperatures show little deviation (typically $< 1^{\circ}\text{C}$) from PI temperatures in the investigated
461 regions (Fig. 2b), suggesting little difference in MH temperature-related weathering. The LGM experiences widespread
462 cooling, which is accentuated at the poles. , increasin the equator-to-pole pressure gradient and consequently
463 strengthens global atmospheric circulation. Despite this global trend, cooling in coastal South Alaska is higher ($\leq 9^{\circ}\text{C}$)
464 than in central Alaska ($0\pm 1^{\circ}\text{C}$). The larger temperature difference in South Alaska geographically coincides with ice
465 cover (Fig. 10b), and should thus be interpreted in context of a different erosional regime. Cooling in most of the lower-
466 latitude regions in South America and central to southeast Asia is relatively mild. The greatest temperature differences
467 in South America are observed for western Patagonia, which was mostly covered by glaciers. The Tibetan plateau
468 experiences more cooling ($3\text{-}5^{\circ}\text{C}$) than adjacent low-altitude regions ($1\text{-}3^{\circ}\text{C}$) during the LGM.

469 The PLIO simulation is generally warmer, and temperature differences are accentuated warming at the poles.
470 Warming in simulation PLIO is greatest in parts of Canada, Greenland and Antarctica (up to 19°C), which
471 geographically coincides with the presence of ice in the PI reference simulation and thus may be attributed to
472 differences in ice cover. It should therefore also be regarded as areas in which process domain shifted from glacial to
473 non-glacial. The warming in simulation PLIO in South Alaska and the US Pacific northwest is mostly uniform and in
474 the range of $1\text{-}5^{\circ}\text{C}$. As before, changes in ice cover reveal that the greatest warming may be associated with the absence
475 of glaciers relative to the PI simulation. Warming in South America is concentrated at the Pacific west coast and the
476 Andes between Lima and Chiclayo, and along the Chilean-Argentinian Andes south of Bolivia ($\leq 9^{\circ}\text{C}$).

477 Overall, annual mean temperatures in the MH simulation show little deviation from PI values. The more

478 significant temperature deviations of the colder LGM and of the warmer PLIO simulations are accentuated at the poles
479 leading to higher and lower equator-to-pole temperature gradients respectively. The largest temperature-related changes
480 (relative to PI conditions) in weathering and subsequent erosion, in many cases through a shift in the process domain
481 from glacial to non-glacial or vice versa, are therefore to be expected in the LGM and PLIO climates.

482

483 **4.1.2 Temperature comparison to other studies**

484 LGM cooling is accentuated at the poles, thus increases the equator-to-pole pressure gradient and consequently
485 strengthens global atmospheric circulation, and is in general agreement with studies such as Otto-Bliesner et al. [2006]
486 and Braconnot et al. [2007]. The PLIO simulation shows little to no warming in the tropics and accentuated warming at
487 the poles, as do findings of Salzmann et al. [2011] and Robinson [2009] and Ballantyne [2010] respectively. This would
488 reduce the equator-to-pole sea and land surface temperature gradient, as also reported by Dowsett et al. [2010], and also
489 weaken global atmospheric circulation. Agreement with proxy-based reconstructions, as is the case of the relatively
490 little warming in lower latitudes, is not surprising given that sea surface temperature reconstructions (derived from
491 previous coarse resolution coupled ocean-atmosphere models) are prescribed in this uncoupled atmosphere simulation.
492 It should be noted that coupled ocean-atmosphere simulations do predict more low-latitude warming [e.g. Stepanek and
493 Lohmann 2012; Zhang et al. 2013b]. The PLIO warming in parts of Canada and Greenland (up to 19°C) and consistent
494 with values based on multi-proxy studies [Ballantyne et al., 2010]. Due to a scarcity of palaeobotanical proxies in
495 Antarctica, reconstruction-based temperature and ice-sheet extent estimates for a PLIO climate have high uncertainties
496 [Salzmann et al., 2011], making model validation difficult. Furthermore, controversy about relatively little warming in
497 the south polar regions compared to the north polar regions remains [e.g. Hillenbrand and Fütterer, 2002; Wilson et al.,
498 2002]. Mid-latitude PLIO warming is mostly in the 1-3°C range with notable exceptions of cooling in the northern
499 tropics of Africa and on the Indian subcontinent, especially south of the Himalayan orogen.

500

501 **4.2 Synthesis of precipitation changes**

502

503 **4.2.1 Precipitation and implications for weathering and erosion**

504 Changes in precipitation affects erosion through river incision, sediment transport, and erosion due to extreme
505 precipitation events and storms [e.g. Whipple and Tucker, 1999; Hobbey et al., 2010]. Furthermore, vegetation type and
506 cover also co-evolve with variations in precipitation and with changes in geomorphology [e.g. Marston 2010; Roering
507 et al., 2010]. These vegetation changes in turn modify hillslope erosion by increasing root mass and canopy cover, and
508 decreasing water-induced erosion via surface runoff [e.g. Gyssels et al., 2005]. Therefore, understanding and
509 quantifying changes in precipitation in different palaeoclimates is necessary for a more complete reconstruction of

510 orogen denudation histories. A synthesis of predicted precipitation changes is provided below, and highlights regions
511 where changes in river discharge and hillslope processes might be impacted by climate change over the last ~3 Ma.

512 Most of North Africa is notably wetter during the MH, which is characteristic of the African Humid Period
513 [Sarnthein 1978]. This pluvial regional expression of the Holocene Climatic Optimum is attributed to sudden changes in
514 the strength of the African monsoon caused by orbital-induced changes in summer insolation [e.g. deMenocal et al.
515 2000]. Southern Africa is characterised by a wetter climate to the east and drier climate to the west of the approximate
516 location of the Congo Air Boundary (CAB), the migration of which has previously been cited as a cause for
517 precipitation changes in East Africa [e.g. Juninger et al. 2014]. In contrast, simulated MH precipitation rates show little
518 deviation from the PI in most of the investigated regions, suggesting little difference in MH precipitation-related
519 erosion. The Himalayan orogen is an exception and shows a precipitation increase of up to 2000 mm/a. The climate's
520 enhanced erosion potential, that could result from such a climatic change, should be taken into consideration when
521 palaeo-erosion rates estimated from the geological record in this area are interpreted [e.g. Bookhagen et al., 2005].
522 Specifically, higher precipitation rates (along with differences in other rainfall-event parameters) could increase the
523 probability of mass movement events on hillslopes, especially where hillslopes are close to the angle of failure [e.g.
524 Montgomery, 2001], and modify fluxes to increase shear stresses exerted on river beds and increase stream capacity to
525 enhance erosion on river beds (e.g. by abrasion).

526 Most precipitation on land is decreased during the LGM due to large-scale cooling and decreased evaporation
527 over the tropics, resulting in an overall decrease in inland moisture transport [e.g., Braconnot et al. 2007]. North
528 America, south of the continental ice sheets, is an exception and experiences increases in precipitation. For example, the
529 investigated US Pacific Northwest and the southeastern coast of Alaska experience experience strongly enhanced
530 precipitation of ≤ 1700 mm/a and ≤ 2300 mm/a, respectively. These changes geographically coincide with differences in
531 ice extent. An increase in precipitation in these regions may have had direct consequences on the glaciers' mass balance
532 and equilibrium line altitudes, where the glaciers' effectiveness in erosion is highest [e.g. Egholm et al., 2009; Yanites
533 and Ehlers, 2012]. The differences in the direction of precipitation changes, and accompanying changes in ice cover
534 would likely result in more regionally differentiated variations in precipitation-specific erosional processes in the St.
535 Elias Range rather than causing systematic offsets for the LGM. Although precipitation is significantly reduced along
536 much of the Himalayan orogen (≤ 1600 mm/a), , northeast India experiences strongly enhanced precipitation (≤ 1900
537 mm/a). This could have large implications for studies of uplift and erosion at orogen syntaxes, where highly localized
538 and extreme denudation has been documented [e.g. Koons et al., 2013; Bendick and Ehlers, 2014].

539 Overall, the PLIO climate is wetter than the PI climate, in particular in the (northern) mid-latitudes, and possibly
540 related to a northward shift of the northern Hadley cell boundary that is ultimately the result of a reduced equator-to-
541 pole temperature gradient [e.g. Haywood et al. 2000, 2013; Dowsett et al. 2010]. Most of the PLIO precipitation over

542 land increases , esp. at the Himalayan orogen by ≤ 1400 mm/a, and decreases from eastern Nepal to Namcha Barwa
543 (≤ 2500 mm/a). Most of the Atacama Desert experiences an increase in precipitation by 100-200 mm/a, which may have
544 to be considered in erosion and uplift history reconstructions for the Andes. A significant increase (~ 2000 mm/a) in
545 precipitation from simulation PLIO to modern conditions is simulated for the eastern margin of the Andean Plateau in
546 Peru and for northern Bolivia. This is consistent with recent findings of a pulse of canyon incision in these locations in
547 the last ~ 3 Ma [Lease and Ehlers, 2013].

548 Overall, the simulated MH precipitation varies least from PI precipitation. The LGM is generally drier than the
549 PI simulation, even though pockets of a wetter-than-PI climate do exist, such as much of coastal North America. Extra-
550 tropical increased precipitation of the PLIO simulation and decreased precipitation of the LGM climate may be the
551 result of decreased and increased equator-to-pole temperature gradients, respectively.

552

553 **4.2.2 Precipitation comparison to other studies**

554 The large scale LGM precipitation decrease on land, related to cooling and decreased evaporation over the
555 tropics, and greatly reduced precipitation along much of the Himalayan orogeny, is consistent with previous studies by,
556 (for example) Braconnot et al. [2007]. The large scale PLIO precipitation increase due to a reduced equator-to-pole
557 temperature gradient, has previously been pointed out by e.g. Haywood et al. [2000, 2013] and Dowsett et al. [2010]. A
558 reduction of this gradient by ca. 5°C is indeed present in the PLIO simulation of this study (Fig. 2b). This precipitation
559 increase over land agrees well with simulations performed at a lower spatial model resolution [cf. Stepanek and
560 Lohmann, 2012]. Section 4.4 includes a more in-depth discussion of how simulated MH and LGM precipitation
561 differences compare with proxy-based reconstructions in South Asia and South America.

562

563 **4.3 Trends in Late Cenozoic changes in regional climatology**

564 This section describes the major changes in regional climatology and highlights their possible implications on
565 erosion rates.

566

567 *Himalaya-Tibet, South Asia*

568 In South Asia, cluster-analysis based categorization and description of climates (Fig. 6) remains similar
569 throughout time. However, the two wettest climates (C_1 and C_2) are geographically more restricted to the eastern
570 Himalayan orogen in the LGM simulation. Even though precipitation over the South Asia region is generally lower, this
571 shift indicates that rainfall on land is more concentrated in this region and that the westward drying gradient along the
572 orogen is more accentuated than during other time periods investigated here. While there is limited confidence in the
573 global Atmospheric General Circulation Model's abilities to accurately represent meso-scale precipitation patterns [e.g.

574 Cohen 1990], the simulation warrants careful consideration of possible, geographically non-uniform offsets in
575 precipitation in investigations of denudation and uplift histories.

576 MH precipitation and temperature in tropical, temperate and high-altitude South Asia is similar to PI
577 precipitation and temperature, whereas LGM precipitation and temperatures are generally lower (by ca. 100 mm/a and
578 1-2°C respectively), possibly reducing precipitation-driven erosion and enhancing frost-driven erosion in areas pushed
579 into a near-zero temperature range during the LGM.

580

581 *Andes, South America*

582 Clusters in South America (Fig. 9), which are somewhat reminiscent of the Köppen and Geiger classification
583 [Kraus, 2001], remain mostly the same over the last 3 Ma. In the PLIO simulation, the lower-altitude east of the region
584 is characterized by four distinct climates, which suggests enhanced latitudinal variability in the PLIO climate compared
585 to PI with respect temperature and precipitation.

586 The largest temperature deviations from PI values are derived for the PLIO simulation in the (tropical and
587 temperate) Andes, where temperatures exceed PI values by 5°C. On the other hand, LGM temperatures in the Andes are
588 ca. 2-4°C below PI values in the same region (Fig 7 g and h). In the LGM simulation, tropical South America
589 experiences ca. 50 mm/a less precipitation, the temperate Andes receive ca. 50 mm/a more precipitation than in PI and
590 MH simulations. These latitude-specific differences in precipitation changes ought to be considered in attempts to
591 reconstruct precipitation-specific palaeoerosion rates in the Andes on top of longitudinal climate gradients highlighted
592 by, e.g., Montgomery et al. [2001].

593

594 *St. Elias Range, South Alaska*

595 South Alaska is subdivided into two wetter and warmer clusters in the south, and two drier, colder clusters in the
596 north. The latter are characterised by increased seasonal temperature variability due to being located at higher latitudes
597 (Fig. 12). The different equator-to-pole temperature gradients for LGM and PLIO may affect the intensity of the Pacific
598 North American Teleconnection (PNA) [Barnston and Livzey, 1987], which has significant influence on temperatures
599 and precipitation, especially in southeast Alaska, and may in turn result in changes in regional precipitation and
600 temperature patterns and thus on glacier mass balance. Changes in the Pacific Decadal Oscillation, which is related to
601 the PNA pattern, has previously been connected to differences in Late Holocene precipitation [Barron and Anderson,
602 2011]. While this climate cluster pattern appears to be a robust feature for the considered climate states, and hence over
603 the recent geologic history, the LGM sets itself apart from PI and MH climates by generally lower precipitation (20-40
604 mm) and lower temperatures (3-5°C, Fig. 10, 11), which may favour frost driven weathering during glacial climate
605 states [e.g. Andersen et al., 2015; Marshall et al. 2015] in unglaciated areas, whereas glacial processes would have

606 dominated most of this region as it was covered by ice. Simulation PLIO is distinguished by temperatures that exceed
607 PI and MH conditions by ca. 2°C, and by larger temperature and precipitation value ranges, possibly modifying
608 temperature- and precipitation-dependent erosional processes in the region of South Alaska.

609

610 *Cascade Range, US Pacific Northwest*

611 In all time slices, the geographic climate patterns, based on the cluster analysis (Fig. 15), represents an increase
612 in the degree of continentality from the wetter coastal climates to the further inland located climates with greater
613 seasonal temperature amplitude and lower precipitation and precipitation amplitude (Fig 15 e-h). The most notable
614 difference between the time slices is the strong cooling during the LGM, when temperatures are ca. 13°C (Fig. 13, 14)
615 below those of other time periods. Given that the entire investigated region was covered by ice (Fig 13), we can assume
616 a shift to glacially dominated processes.

617

618 **4.4 Comparison of simulated and observed precipitation differences**

619 The predicted precipitation differences reported in this study were compared with observed (proxy record)
620 palaeoprecipitation change. Proxy based precipitation reconstructions for the MH and LGM are presented for South
621 Asia and South America for the purpose of assessing ECHAM5 model performance, and for identifying inconsistencies
622 between neighbouring proxy data. Due to the repeated glaciations, detailed terrestrial proxy records for the time slices
623 investigated here are not available, to the best of our knowledge, for the Alaskan and Pacific NW USA studies.
624 Although marine records and records of glacier extent are available in these regions, the results from them do not
625 explicitly provide estimates of wetter/drier, or colder/warmer conditions that can be spatially compared to the
626 simulation estimates. For these two areas with no available records, the ECHAM5 predicted results therefore provide
627 predictions from which future studies can formulate testable hypotheses to evaluate.

628 The palaeoclimate changes in terrestrial proxy records compiled here are reported as “wetter than today”, “drier
629 than today” or “the same as today” for each of the study locations, and plotted on top of the simulation-based difference
630 maps as upward facing blue triangles, downward facing red triangles and grey circles respectively (Fig. 16, 17). The
631 numbers listed next to those indicators are the ID numbers assigned to the studies compiled for this comparison and are
632 associated with a citation provided in the figure captions.

633 In South Asia, 14/26 results from local studies agree with the model predicted precipitation changes for the MH.
634 The model seems able to reproduce the predominantly wetter conditions on much of the Tibetan plateau, but predicts
635 slightly drier conditions north of Chengdu, which is not reflected in local reconstructions. The modest mismatch
636 between ECHAM5 predicted and proxy-based MH climate change in south Asia was also documented by Li et al.,
637 [2017], whose simulations were conducted at a coarser (T106) resolution. Despite these model-proxy differences, we

638 note that there are significant discrepancies between the proxy data themselves in neighbouring locations in the MH,
639 highlighting caution in relying solely upon these data for regional palaeoclimate reconstructions. These differences
640 could result from either poor age-constraints in the reported values, or systematic errors in the transfer functions used to
641 convert proxy measurements to palaeoclimate conditions. The widespread drier conditions on the Tibetan Plateau and
642 immediately north of Laos are confirmed by 7/7 of the palaeoprecipitation reconstructions. 23/39 of the reconstructed
643 precipitation changes agree with model predictions for South America during the MH. The model predicted wetter
644 conditions in the central Atacama desert, as well as the drier conditions northwest of Santiago are confirmed by most of
645 the reconstructions. The wetter conditions in southernmost Peru and the border to Bolivia and Chile cannot be
646 confirmed by local studies. 11/17 of the precipitation reconstructions for the LGM are in agreement with model
647 predictions. These include wetter conditions in most of Chile. The most notable disagreement can be seen in northeast
648 Chile at the border to Argentina and Bolivia, where model predicted wetter conditions are not confirmed by reported
649 reconstructions from local sites.

650 Model performance is, in general, higher for the LGM than for the MH and overall satisfactory given that it
651 cannot be expected to resolve sub-grid scale differences in reported palaeoprecipitation reconstructions. However, as
652 mentioned above, it should be noted that some locations (MH of south Asia, and MH of norther Chile) discrepancies
653 exist between neighbouring proxy samples and highlight the need for caution in how these data are interpreted. Other
654 potential sources of error resulting in disagreement of simulated and proxy-based precipitation estimates are the model's
655 shortcomings in simulating orographic precipitation at higher resolutions, and uncertainties in palaeoclimate
656 reconstructions at the local sites. In summary, although some differences are evident in both the model-proxy data
657 comparison and between neighbouring proxy data themselves, the above comparison highlights an overall good
658 agreement between the model and data for the south Asia and South American study areas. Thus, although future
659 advances in GCM model parameterisations and new or improved palaeoclimate proxy techniques are likely, the
660 palaeoclimate changes documented here are found to be in general robust and provide a useful framework for future
661 studies investigating how these predicted changes in palaeoclimate impact denudation.

662

663 **4.5 Conclusions**

664 We present a statistical cluster-analysis-based description of the geographic coverage of possible distinct
665 regional expressions of climates from four different time slices (Fig. 6, 9, 12, 15). These are determined with respect to
666 a selection of variables that characterize the climate of the region and may be relevant to weathering and erosional
667 processes. While the geographic distribution of climate remains similar throughout time (as indicated by results of four
668 different climate states representative for the climate of the last 3 Ma), results for the PLIO simulation suggests more
669 climatic variability east of the Andes (with respect to near-surface temperature, seasonal temperature amplitude,

670 precipitation, seasonal precipitation amplitude and seasonal u-wind and v-wind speeds). Furthermore, the wetter
671 climates in the South Asia region retreat eastward along the Himalayan orogen for the LGM simulation, this is due to
672 decreased precipitation along the western part of the orogen and enhanced precipitation on the eastern end, possibly
673 signifying more localised high erosion rates.

674 Most global trends of the high-resolution LGM and PLIO simulations conducted here are in general agreement
675 with previous studies [Otto-Bliesner et al., 2006; Braconnot et al., 2007; Wei and Lohmann, 2012; Lohmann et al.,
676 2013; Zhang et al., 2013b, 2014; Stepanek and Lohmann, 2012]. The MH does not deviate notably from the PI, the
677 LGM is relatively dry and cool, while the PLIO is comparably wet and warm. While the simulated regional changes in
678 temperature and precipitation usually agree with the sign (or direction) of the simulated global changes, there are
679 region-specific differences in the magnitude and direction. For example, the LGM precipitation of the Tropical Andes
680 does not deviate significantly from PI precipitation, whereas LGM precipitation in the Temperate Andes is enhanced.

681 Comparisons to local, proxy-based reconstructions of MH and LGM precipitation in South Asia and South
682 America reveal satisfactory performance of the model in simulating the reported differences. The model performs better
683 for the LGM than the MH. We note however that compilations of proxy data such as we present here, also identify
684 inconsistencies between neighbouring proxy data themselves, warranting caution in the extent to which both proxy data
685 and palaeoclimate models are interpreted for MH climate change in south Asia, and western South America.

686 The changes in regional climatology presented here are manifested, in part, by small to large magnitude changes
687 in fluvial and hillslope relevant parameters such as precipitation and temperature. For the regions investigated here we
688 find that precipitation differences between the PI, MH, LGM, and PLIO are in many areas around +/- 200-600 mm/yr,
689 and locally can reach maximums of +/- 1000-2000 mm/yr (Figs. 4, 7, 10, 13). In areas where significant precipitation
690 increases are accompanied by changes in ice extent, such as parts of southern Alaska during the LGM, we would expect
691 a shift in the erosional regime to glacier dominated processes. Temperature differences between these same time periods
692 are around 1-4 °C in many places, but reach maximum values of 8-10 °C. Many of these maxima in the temperature
693 differences geographically coincide with changes in ice sheet extent and must therefore be interpreted as part of a
694 different erosional process domains. However, we also observe large temperature differences (~5°C) in unglaciated
695 areas that would be affected by hillslope, frost cracking, and fluvial processes. The magnitude of these differences are
696 not trivial, and will likely impact fluvial and hillslope erosion and sediment transport, as well as biotic and abiotic
697 weathering. The regions of large magnitude changes in precipitation and temperature documented here (Figs. 4, 7, 10,
698 13) offer the highest potential for future observational studies interested in quantifying the impact of climate change on
699 denudation and weathering rates.

700

701

702 **Acknowledgements**

703 The model simulations presented in this study are freely available to interested persons by contacting S. Mutz or T.
704 Ehlers. We note however that the data files are very large (~4 TB, and too large to archive in journal supplementary
705 material) and require familiarity in reading/plotting NetCDF formatted files. European Research Council (ERC)
706 Consolidator Grant number 615703 provided support for S. Mutz. Additional support is acknowledged from the German
707 science foundation (DFG) priority research program 1803 (EarthShape: Earth Surface Shaping by Biota; grants
708 EH329/14-1 and EH329/17-1). We thank B. Adams and J. Starke for constructive discussions. We also thank the
709 reviewers (incl. A. Wickert) for their constructive feedback on this manuscript, which helped to significantly improve it.
710 The DKRZ is thanked for computer time used for some of the simulations presented here. C. Stepanek, M. Werner, and
711 G. Lohmann acknowledge funding by the Helmholtz Climate Initiative Reklim and the Alfred Wegener Institute's
712 research programme Marine, Coastal and Polar Systems.

713

714

715 **Figure Captions**

716

717 **Figure 1** Topography for regions (a) tropical South Asia, (b) temperate South Asia, (c) high altitude South Asia, (d)
718 temperate South America, (e) tropical South America, (f) temperate Andes, (g) tropical Andes, SE Alaska and Casca-
719 dia.

720 **Figure 2** Global PI annual mean near-surface temperatures (a), and deviations of MH, LGM and PLIO annual mean
721 near-surface temperatures from PI values (b). Units are °C and insignificant ($p < 99\%$) differences (as determined by
722 a t-test) are greyed out.

723 **Figure 3** Global PI annual mean precipitation (a), and deviations of MH, LGM and PLIO annual mean near-surface
724 temperatures from PI values (b). Units are mm/yr.

725 **Figure 4** PI annual mean near-surface temperatures (a), and deviations of MH, LGM and PLIO annual mean near-sur-
726 face temperatures from PI values (b) for the South Asia region. Insignificant ($p < 99\%$) differences (as determined
727 by a t-test) are greyed out.

728 **Figure 5** PI, MH, LGM and PLIO annual mean precipitation in (a) tropical South Asia, (b) temperate South Asia, and
729 (c) high-altitude South Asia; PI, MH, LGM and PLIO annual mean temperatures in (d) tropical South Asia, (e) tem-

730 perate South Asia, and (f) high-altitude South Asia. For each time slice, the minimum, lower 25th percentile, median,
731 upper 75th percentile and maximum are plotted.

732 **Figure 6** Geographical coverage and characterization of climate classes C₁- C₆ based on cluster-analysis of 8 variables
733 (near surface temperature, seasonal near surface temperature amplitude, total precipitation, seasonal precipitation
734 amplitude, u-wind in January and July, v-wind in January and July) in the South Asia region. The geographical cov-
735 erage of the climates C₁- C₆ is shown on the left for PI (a), MH (b), LGM (c) and PLIO (d); the complementary,
736 time-slice specific characterization of C₁- C₆ for PI (e), MH (f), LGM (g) and PLIO (h) is shown on the right.

737 **Figure 7** PI annual mean near-surface temperatures (a), and deviations of MH, LGM and PLIO annual mean near-sur-
738 face temperatures from PI values (b) for western South America. Insignificant (p < 99%) differences (as determined
739 by a t-test) are greyed out.

740 **Figure 8** PI, MH, LGM and PLIO annual mean precipitation in (a) tropical South America, (b) temperate South Amer-
741 ica, (c) tropical Andes, and (d) temperate Andes; PI, MH, LGM and PLIO annual mean temperatures in (e) tropical
742 South America, (f) temperate South America, (g) tropical Andes, and (h) temperate Andes. For each time slice, the
743 minimum, lower 25th percentile, median, upper 75th percentile and maximum are plotted.

744 **Figure 9** Geographical coverage and characterization of climate classes C₁- C₆ based on cluster-analysis of 8 variables
745 (near surface temperature, seasonal near surface temperature amplitude, precipitation, seasonal precipitation amp-
746 litude, u-wind in January and July, v-wind in January and July) in western South America. The geographical cover-
747 age of the climates C₁- C₆ is shown on the left for PI (a), MH (b), LGM (c) and PLIO (d); the complementary, time-
748 slice specific characterization of C₁- C₆ for PI (e), MH (f), LGM (g) and PLIO (h) is shown on the right.

749 **Figure 10** PI annual mean near-surface temperatures (a), and deviations of MH, LGM and PLIO annual mean near-sur-
750 face temperatures from PI values (b) for the South Alaska region. Insignificant (p < 99%) differences (as determined
751 by a t-test) are greyed out.

752 **Figure 11** PI, MH, LGM and PLIO annual mean precipitation (a), and mean annual temperatures (b) in South Alaska.
753 For each time slice, the minimum, lower 25th percentile, median, upper 75th percentile and maximum are plotted.

754 **Figure 12** Geographical coverage of climate classes C₁- C₄ based on cluster-analysis of 4 variables (near surface tem-
755 perature, seasonal near surface temperature amplitude, total precipitation, seasonal total precipitation amplitude) in
756 southern Alaska. The geographical coverage of the climates C₁- C₄ is shown on the left for PI (a), MH (b), LGM (c)

757 and PLIO (d); the complementary, time-slice specific characterization of C₁- C₆ for PI (e), MH (f), LGM (g) and
758 PLIO (h) is shown on the right.

759 **Figure 13** PI annual mean near-surface temperatures (a), and deviations of MH, LGM and PLIO annual mean near-sur-
760 face temperatures from PI values (b) for the US Pacific Northwest. Insignificant (p < 99%) differences (as determ-
761 ined by a t-test) are greyed out.

762 **Figure 14** PI, MH, LGM and PLIO annual mean precipitation (a), and annual mean temperatures (b) in the Cascades,
763 US Pacific Northwest. For each time slice, the minimum, lower 25th percentile, median, upper 75th percentile and
764 maximum are plotted.

765 **Figure 15** Geographical coverage and characterization of climate classes C₁- C₄ based on cluster-analysis of 4 variables
766 (near surface temperature, seasonal near surface temperature amplitude, total precipitation, seasonal total precipita-
767 tion amplitude) in the Cascades, US Pacific Northwest. The geographical coverage of the climates C₁- C₄ is shown
768 on the left for PI (a), MH (b), LGM (c) and PLIO (d); the complementary, time-slice specific characterization of C₁-
769 C₆ for PI (e), MH (f), LGM (g) and PLIO (h) is shown on the right.

770 **Figure 16** Simulated annual mean precipitation deviations of MH (left) and LGM (right) from PI values in South Asia,
771 and temporally corresponding proxy-based reconstructions, indicating wetter (upward facing blue triangles), drier
772 (downward facing red triangles) or similar (grey circles) conditions in comparison with modern climate. MH proxy-
773 based precipitation differences are taken from Mügler et al. (2010) (66), Wischnewski et al. (2011) (67), Mischke et
774 al. (2008), Wischnewski et al. (2011), Herzsuh et al. (2009) (68), Yanhong et al. (2006) (69), Morrill et al. (2006)
775 (70), Wang et al. (2002) (71), Wuennemann et al. (2006) (72), Zhang et al. (2011), Morinaga et al. (1993),
776 Kashiwaya et al. (1995) (73), Shen et al. (2005) (74), Liu et al. (2014) (75), Herzsuh et al. (2006) (76), Zhang and
777 Mischke (2009) (77), Nishimura et al. (2014) (78), Yu and Lai (2014) (79), Gasse et al. (1991) (80), Van Campo et
778 al. (1996) (81), Demske et al. (2009) (82), Kramer et al. (2010) (83), Herzsuh et al. (2006) (84), Hodell et al.
779 (1999)(85), Hodell et al. (1999) (86), Shen et al. (2006) (87), Tang et al. (2000) (88), Tang et al. (2000) (89), Zhou et
780 al. (2002) (90), Liu et al. (1998) (91), Asashi (2010)(92), Kotila et al. (2009) (93), Kotila et al. (2000) (94), Wang et
781 al. (2002) (95), Hu et al. (2014) (96), Hodell et al. (1999) (97), Hodell et al. (1999) (98).

782 **Figure 17** Simulated annual mean precipitation deviations of MH (left) and LGM (right) from PI values in South Amer-
783 ica, and temporally corresponding proxy-based reconstructions, indicating wetter (upward facing blue triangles),
784 drier (downward facing red triangles) or similar (grey circles) conditions in comparison with modern climate. MH

785 proxy-based precipitation differences are taken from Bird et al. (2011) (1), Hansen et al (1994) (2), Hansen et al
786 (1994) (3), Hansen et al (1994) (4), Hansen et al (1994) (5), Hansen et al (1994) (6), Hillyer et al. (2009) (7),
787 D'Agostino et al. (2002) (8), Baker et al. (2001) (9), Schwalb et al (1999) (10), Schwalb et al (1999) (11), Schwalb
788 et al (1999) (12), Schwalb et al (1999) (13), Moreno et al (2009) (14), Pueyo et al (2011) (15), Mujica et al (2015)
789 (16), Fritz et al. (2004) (17), Gayo et al. (2012) (18), Latorre et al. (2006) (19), Latorre et al. (2003) (20), Quade et al
790 (2008) (21), Bobst et al. (2001) (22), Grosjean et al. (2001) (23), Betancourt et al. (2000) (24), Latorre et al. (2002)
791 (25), Rech et al. (2003) (26), Diaz et al. (2012) (27), Maldonado et al (2005) (28), Diaz et al. (2012) (29), Lamy et
792 al. (2000) (30), Kaiser et al. (2008) (31), Maldonado et al. (2010) (32), Villagrán et al. (1990) (33), Méndez et al.
793 (2015) (34), Maldonado et al. (2006) (35), Lamy et al. (1999) (36), Jenny et al. (2002) (37), Jenny et al. (2002b)
794 (38), Villa-Martínez et al. (2003) (39), Bertrand et al. (2008) (40), De Basti et al. (2008) (41), Lamy et al. (2009)
795 (42), Lamy et al. (2002) (43), Szeicz et al. (2003) (44), de Porras et al. (2012) (45), de Porras et al. (2014) (46),
796 Markgraf et al. (2007) (47), Siani et al. (2010) (48), Gilli et al. (2001) (49), Markgraf et al. (2003) (50), Stine et al.
797 (1990) (51).

798

799

800 **References**

801

802 Abe-Ouchi, A., Saito, F., Kageyama, M., Bracannot, P., Harrison, S. P., Lambeck, K., Otto-Bliesner, B. L., Peltier, W.R.,
803 Tarasov, L., Peterschmitt, J.-Y., Takahashi, K.: Ice-sheet configuration in the CMUP5/PMIP3 Last Glacial Maximum
804 experiments. *Geosci. Model Dev.*, 8, 3621-3637, doi:10.5194/gmd-8-3621-2015, 2015

805 Andersen, J., Egholm, D.L., Knudsen, M.F., Jansen, J., Nielsen, S.B., The periglacial engine of mountain erosion – Part
806 1: Rates of frost cracking and frost creep., *Earth Surface Dynamics*, 3(4), 447-462, 2015.

807 Arnold, L., Breon, F.M., and Brewer, S: The earth as an extrasolar planet: the vegetation spectral signature today and
808 during the last Quaternary climatic extrema, *Int. J. Astrobiol.*, 8, 81–94.
809 <http://dx.doi.org/10.1017/S1473550409004406>, 2009.

810 Asahi, K.: Equilibrium-line altitudes of the present and Last Glacial Maximum in the eastern Nepal Himalayas and
811 their implications for SW monsoon climate, *Quatern. Int.*, 212, 26-34, doi:10.1016/j.quaint.2008.08.004, 2010.

812 Bahrenberg, G., Giese, E., and Nipper, J.: Multivariate Statistik. *Statistische Methoden in der Geographie 2*, Stuttgart,
813 1992.

814 Baker, P. A., Seltzer, G. O., Fritz, S. C., Dunbar, R. B., Grove, M. J., Tapia, P. M., Cross L., Rowe H. D., and Baroda, J.
815 P.: The History of South America Tropical Precipitation for the Past 25,000 Years, *Earth and Atmospheric Sciences*,

- 816 291, 640-643, doi:10.1126/science.291.5504.640, 2001.
- 817 Ballantyne, A.P., Greenwood, D.R., Sinninghe Damste, J.S., Csank, A.Z., Eberle, J.J., and Rybczynski, N.: Significantly
818 warmer Arctic surface temperatures during the Pliocene indicated by multiple independent proxies, *Geology* 38 (7),
819 603–606, 2010.
- 820 Banfield, J.F., Barker, W.W., Welch, S.A., and Taunton, A.: Biological impact on mineral dissolution: application of the
821 lichen model to understanding mineral weathering in the rhizosphere, *Proceedings of the National Academy of*
822 *Sciences*, 96, 3404-3411, 1999.
- 823 Barnston, A. G. and Livezey, R. E.: Classification, Seasonality and Persistence of Low-Frequency Atmospheric
824 Circulation Patterns, *Mon. Weather Rev.*, 115, 1083-1126, doi:10.1175/1520-
825 0493(1987)1151083:CSAPOL2.0.CO;2, 1987.
- 826 Barron, J.A., and Anderson, L.: Enhanced Late Holocene ENSO/PDO expression along the margins of the eastern North
827 Pacific. *Quaternary International*, 235, 3-12, 2011.
- 828 Bendick, R., and Ehlers, T.A.: Extreme localized exhumation at syntaxes initiated by subduction geometry, *Geophys.*
829 *Res. Lett.*, 41(16), 2014GL061026, doi:10.1002/2014GL061026, 2014.
- 830 Bertrand, S., Charlet F., Charlier B., Renson V., and Fagel N.: Climate variability of southern Chile since the Last
831 Glacial Maximum: a continuous sedimentological records from Lago Puyehue (40°S), *J. Paleolimnol.*, 39, 179-195,
832 doi:10.1007/s10933-007-9117-y, 2008.
- 833 Betancourt, J. L., Latorre C., Rech J. A., Quade J., and Rylander K,A.: A 22,000 Year Record of Monsoonal Precipita-
834 tion from Northern Chile's Atacama Desert, *Science*, 289, 1542-1546, doi: 10.1126/science.289.5484.1542, 2000.
- 835 Bigelow, N. H., Brubaker, L. B., Edwards, M. E., Harrison, S. P., Prentice, I. C., Anderson, P. M., Andreev, A. A.,
836 Bartlein, P. J., Christensen, T. R., Cramer, W., Kaplan, J. O., Lozhkin, A. V., Matveyeva, N. V., Murray, D. V.,
837 McGuire, A. D., Razzhivin, V. Y., Ritchie, J. C., Smith, B., Walker, D. A., Gajewski, K., Wolf, V., Holmqvist, B. H.,
838 Igarashi, Y., Kremenetskii, K., Paus, A., Pisaric, M. F. J., and Vokova, V. S.: Climate change and Arctic ecosystems
839 I. Vegetation changes north of 55°N between the last glacial maximum, mid-Holocene and present. *Journal of Geo-*
840 *physical Research - Atmospheres*, 108(D19), doi: 10.1029/2002JD002558, 2003.
- 841 Bird, B. W., Abbott M .B., Rodbell D. T., and Vuille M.: Holocene tropical South American hydroclimate revealed from
842 a decadal resolved lake sediment $\delta^{18}\text{O}$ record, *Earth Planet. Sc. Lett.*, 310, 192-202,
843 doi:10.1016/j.epsl.2011.08.040, 2011.
- 844 Bobst, A. L., Lowenstein, T. K., Jordan, T. E., Godfrey, L. V., Ku, T.-L., and Luo, S.: A 106 ka paleoclimate record from
845 drill core of the Salar de Atacama, northern Chile, *Palaeogeogr. Palaeocl.*, 173, 21-42, doi:10.1016/S0031-
846 0182(01)00308, 2001.
- 847
848 Braconnot, P., Otto-Bleisner, B., Harrison, S.P., Joussaume, S., Peterschmitt, J.-Y., Abe-Ouchi, A., Crucifix, M.,
849 Driesschaert, E., Fichetfet, T., Hewitt, C.D., Kagayama, M., Kitoh, A., Loutre, M.-F., Marti, O., Merkel, U.,
850 Ramstein, G., Valdes, P., Weber, L., Yu, Y., and Zhao, Y.: Results of PMIP2 coupled simulations of the mid-
851 Holocene and Last Glacial maximum, part 1: experiments and large-scale features, *Clim Past* 3:261–277, 2007.

- 852 Bohner, J.: General climatic controls and topoclimatic variations in Central and High Asia, *Boreas*, 35(2), 279-295,
853 2006.
- 854 Bookhagen, B., Thiede, R.C., and Strecker, M.R.: Late Quaternary intensified monsoon phases control landscape
855 evolution in the northwest Himalaya, *Geology*, 33(2), 149-152. doi: 10.1130/G20982.1, 2005.
- 856 Boos, W. R., and Kuang, Z.: Dominant control of the South Asian monsoon by orographic insulation versus plateau
857 heating, *Nature*, 463, 218-222, 2010.
- 858 Braun, J.: A simple model for regolith formation by chemical weathering: Regolith Formation, *Journal of Geophysical*
859 *Research Earth's Surface*, DOI: 10.1002/2016JF003914, 2016.
- 860 Caves, J.: Late Miocene Uplift of the Tian Shan and Altai and Reorganization of Central Asia Climate, *GSA Today*,
861 doi:10.1130/gsatg305a.1, 2017.
- 862 CLIMAP Project Members: Seasonal Reconstruction of the Earth's Surface at the Last Glacial Maximum.
863 *Map and Chart Series*, Vol. 36, Geological Society of America, 18 pp., 1981.
864
- 865 Cohen, S.J.: Bringing the global warming issue close to home: The challenge of regional impact studies. *Bulletin of the*
866 *American Meteorological Society*, 71: 520 – 526., 1990.
- 867 D'Agostino, K., Seltzer, G., Baker, P., Fritz, S., and Dunbar, R.: Late-Quaternary lowstands of Lake Titicaca: evidence
868 from high-resolution seismic data, *Palaeogeogr. Palaeoclimatol.*, 179, 97-111, doi:10.1016/S0031-0182(01)00411-4, 2002.
- 869 De Batist, M., Fagel N., Loutre M. F., and Chapron E.: A 17,900-year multi-proxy lacustrine record of Lago Puyehue
870 (Chilean Lake District): introduction, *J. Paleolimnol.*, 39, 151-161, doi:10.1007/s10933-007-9113-2, 2007.
- 871 de Porras, M. E., Maldonado, A., Abarzua, A. M., Cardenas, M. L., Francois, J. P., Martel-Cea, A., Stern, C. R.,
872 Mendez, C., and Reyes, O.: Postglacial vegetation, fire and climate dynamics at Central Chilean Patagonia (Lake
873 Shaman, 44°S), *Quaternary Sci. Rev.*, 50, 71-85, doi:10.1016/j.quascirev.2012.06.015; 2012.
- 874 de Porras, M. E., Maldonado, A., Quintana, F. A., Martel-Cea, A., Reyes, O., and Méndez, C.: Environmental and cli-
875 matic changes in central Chilean Patagonia since the Late Glacial (Mallín El Embudo, 44° S), *Clim. Past*, 10, 1063–
876 1078, doi:10.5194/cp-10-1063-2014, 2014.
- 877 Delunel, R., van der Beek, P. A., Carcaillet, J., Bourlès, D. L., and Valla, P.G.: Frost-cracking control on catchment de-
878 nudation rates: Insights from in situ produced ¹⁰Be concentrations in stream sediments (Ecrins–Pelvoux massif,
879 French Western Alps), *Earth and Planetary Science Letters*, 293(1–2), 72–83, doi:10.1016/j.epsl.2010.02.020, 2010.
- 880 DeMenocal, P., Ortiz, J., Guilderson, T., Adkins, J., Samthein, M., Baker, L., and Yarusinsky, M.: Abrupt onset and ter-
881 mination of the African Humid Period: rapid climate responses to gradual insolation forcing, *Quaternary Sci. Rev.*,
882 19, 347-361, doi:10.1016/S0277-3791(99)00081-5, 2000.
- 883 Demske, D., Tarasov, P. E., Wünnemann, B., and Riedel, F.: Late glacial and Holocene vegetation, Indian monsoon and
884 westerly circulation in the Trans-Himalaya recorded in the lacustrine pollen sequence from Tso Kar, Ladakh, NW
885 India, *Palaeogeogr. Palaeoclimatol.*, 279, 172-185, doi:10.1016/j.palaeo.2009.05.008, 2009.
- 886 Diaz, F.P., Latorre, C., Maldonado, A., Quade, J., and Betancourt, J.L.: Rodent middens reveal episodic, long-distance

887 plant colonizations across the hyperarid Atacama Desert over the last 34,000 years, *J. Biogeogr.*, 39, 510-525,
888 doi:10.1111/j.1365-2699.2011.02617.x, 2012.

889 Dietrich, W. E., and Perron, J.T.: The search for a topographic signature of life, *Nature*, 439(7075), 411–418,
890 doi:10.1038/nature04452, 2006.

891 Dietrich, S., Werner, M., Spanghel, T., and Lohmann, G.: Influence of orbital forcing and solar activity on water iso-
892 topes in precipitation during the mid and late Holocene, *Clim. Past*, 9, 13-26. doi:10.5194/cp-9-13-2013, 2013.
893

894 Dettman, D.L., Fang, X.M., Garziona, C.N., and Li, J.J.: Uplift-driven climate change at 12 Ma: a long delta O-18 re-
895 cord from the NE margin of the Tibetan plateau. *Earth and Planetary Science Letters*, 214(1-2), 267-277, 2003.

896 Dowsett, H.J., Robinson, M., Haywood, A., Salzmann, U., Hill, D., Sohl, L., Chandler, M., Williams, M., Foley, K.,
897 and Stoll, D.: The PRISM3D paleoenvironmental reconstruction. *Stratigraphy*, 7, 123–139, 2010.

898 Egholm, D.L., Nielsen, S.B., Pedersen, V.K., Lesemann, J.: Glacial effects limiting mountain height, *Nature*, 460(7257),
899 884-887, 2009.

900 Ehlers, T.A., and Poulsen, C.J.: Influence of Andean uplift on climate and paleoaltimetry estimates, *Earth and Planet-
901 ary Science Letters*, 281(3-4), 238-248, 2009.

902 Etheridge, D.M., Steele, L., Langenfelds, R., Francey, R., Barnola, J., and Morgan, V.: Natural and anthropogenic
903 changes in atmospheric CO₂ over the last 1000 years from air in Antarctic ice and firn, *J Geophys Res* 101:4115–
904 4128, 1996.
905

906 Etheridge, D.M., L. Steele, R. Francey, and R. Langenfelds (1998), Atmospheric methane between 1000 a.d. and
907 present: evidence of anthropogenic emissions and climatic variability. *J Geophys Res*, 103:15979–15993
908

909 Feng, R., Poulsen, C.J., Werner, M., Chamberlain, C.P., Mix, H.T., and Mulch, A.: Early Cenozoic evolution of topo-
910 graphy, climate, and stable isotopes in precipitation in the North American Cordillera, *American Journal of Science*,
911 313(7), 613–648, 2013.

912 Feng, R., Poulsen, C.J., Werner, M., 2016. Tropical circulation intensification and tectonic extension recorded
913 by Neogene terrestrial δ18O records of the western United States. *Geology* 44. doi:10.1130/G38212.1
914

915 Feng, R., Poulsen, C.J., 2016. Refinement of Eocene lapse rates, fossil-leaf altimetry, and North American
916 Cordilleran surface elevation estimates. *Earth Planet. Sci. Lett.* doi:10.1016/j.epsl.2015.12.022
917

918 Fritz, S. C., Baker, P. A., Lowenstein, T. K., Seltzer, G. O., Rigsby, C. A., Dwyer, G. S., Tapia, P. M., Arnold, K.
919 K., Ku, T. L., and Luo, S: Hydrologic variation during the last 170,000 years in the southern hemisphere
920 tropics of South America, *Quaternary Res.*, 61, 95 – 104, doi:10.1016/j.yqres.2003.08.007, 2004. Gasse, F.,
921 Arnold, M., Fontes, J. C., Fort, M., Gibert, E., Huc, A., Li, B., Li, Y., Liu, Q., Melleres, F., Van Campo, E., Wang, F.,
922 and Zhang, Q.: A 13,000-year climate record from western Tibet, *Nature*, 353, 742-745,
923 doi:10.1016/j.quaint.2006.02.001, 1991.

924 Gayo E. M., Latorre, C., Santoro, C. M., Maldonado, A., and De Pol-Holz, R.: Hydroclimate variability in the low-elev-
925 ation Atacama Desert over the last 2500 yr, *Clim. Past*, 8, 287-306, doi:10.5194/cp-8-287-2012, 2012. Gierz, P.,
926 Lohmann, G., and Wei, W.: Response of Atlantic Overturning to future warming in a coupled atmosphere-ocean-ice

- 927 sheet model, *Geophysical Research Letters*, 42, 6811-6818, doi:10.1002/2015GL065276, 2015.
- 928 Gilli, A., Ariztegui, D., Bradbury, J. P., Kelts, K. R., Markgraf, V., and McKenzie, J. A.: Tracking abrupt climate change
929 in the Southern Hemisphere: a seismic stratigraphic study of Lago Cardiel, Argentina (49°S), *Terra Nova*, 13, 443-
930 448, doi:10.1046/j.1365-3121.2001.00377.x, 2001.
- 931 Glotzbach, C., van der Beek, P., Carcaillet, J., and Delunel, R.: Deciphering the driving forces of erosion rates on mil-
932 lennial to million-year timescales in glacially impacted landscapes: An example from the Western Alps, *Journal of*
933 *Geophysical Research: Earth Surface*, 118, 1491-1515, 2013.
- 934 Gong, X., Knorr, G., Lohmann, G., and Zhang, X.: Dependence of abrupt Atlantic meridional ocean circulation changes
935 on climate background states, *Geophysical Research Letters*, 40 (14), 3698-3704, doi:10.1002/grl.50701, 2013.
- 936 Grosjean, M., Van Leeuwen, J., Van der Knaap, W., Geyh, M., Ammann, B., Tanner, W., Messerli, B., Núñez, L.,
937 Valero-Garcés, B., and Veit, H. : A 22,000 14C year BP sediment and pollen record of climate change from Laguna
938 Miscanti (23°S), northern Chile, *Global Planet. Change*, 28, 35–51, doi:10.1016/S0921-8181(00)00063-1, 2001.
- 939 Gyssels, G., Poesen, J., Bochet, E., and Li, Y.: Impact of plant roots on the resistance of soils to erosion by water: a re-
940 view, *Progress in Physical Geography*, 29, 189–217. <http://doi.org/10.1191/0309133305pp443ra>, 2005.
- 941 Hansen, B. C. S., Seltzer, G. O., and Wright Jr., H.E.: Late Quaternary vegetational change in the central Peruvian
942 Andes, *Palaeogeogr. Palaeoclimatol.*, 109, 263-285, doi:10.1016/0031-0182(94)90179-1, 1994.
- 943 Harris, I., Jones, P.D., Osborn, T.J., and Lister, D.H.: Updated high-resolution grids of monthly climatic observations -
944 the CRU TS3.10 Dataset, *International Journal of Climatology*, doi:10.1002/joc.3711, 2013.
- 945 Harrison, S. P., Yu, G., Takahara, H., and Prentice, I. C.: Palaeovegetation - Diversity of temperate plants in east Asia.
946 *Nature* 413, 129-130, 2001.
947
- 948 Harrison, S.P., Bartlein, P.J., Brewer, S., Prentice, I.C., Boyd, M., Hessler, I., Holmgren, K., Izumi, K., and Willis, K.:
949 Climate model benchmarking with glacial and mid-Holocene climates, *Climate Dynamics*, 43, 671-688. doi
950 10.1007/s00382-013-1922-6, 2013.
- 951 Haywood, A.M., Valdes, P.J., and Sellwood, B.W.: Global scale palaeoclimate reconstruction of the middle Pliocene cli-
952 mate using the UKMO GCM: initial results. *Global and Planetary Change*, 25 (3–4), 239–256, 2000.
- 953 Haywood, A.M., Dowsett, H.J., Otto-Bliesner, B., Chandler, M.A., Dolan, A.M., Hill, D.J., Lunt, D.J., Robinson, M.M.,
954 Rosenbloom, N., Salzmann, U., and Sohl, L.E.: Pliocene Model Intercomparison Project (PlioMIP): experimental
955 design and boundary conditions (Experiment 1), *Geoscientific Model Development* (3), 227-242, 2010.
956
- 957 Haywood, A.M., Hill, D.J., Dolan, A.M., Otto-Bliesner, B., Bragg, F., Chan, W.-L., Chandler, M.A., Contoux, C., Jost,
958 A., Kamae, Y., Lohmann, G., Lunt, D.J., Abe-Ouchi, A., Pickering, S.J., Ramstein, G., Rosenbloom, N.A., Sohl, L.,
959 Stepanek, C., Yan, Q., Ueda, H., and Zhang, Z.: Large-scale features of Pliocene climate: results from the Pliocene
960 Model Intercomparison Project, *Clim. Past*, 9, 191-209. doi:10.5194/cp-9-191-2013, 2013.
961

- 962 Herman, F., Seward, D., Valla, P.G., Carter, A., Kohn, B., Willett, S.D., and Ehlers, T.A.: Worldwide acceleration of
963 mountain erosion under a cooling climate, *Nature*, 504, 423–426. doi:10.1038/nature12877, 2013.
- 964 Herzsuh, U., Kuerschner, H., and Mischke, S.: Temperature variability and vertical vegetation belt shifts during the
965 last ~50,000 yr in the Qilian Mountains (NE margin of the Tibetan Plateau, China), *Quaternary Res.*, 66, 133-146,
966 doi:10.1016/j.yqres.2006.03.001, 2006a.
- 967 Herzsuh, U., Winter, K., Wuennemann, B., and Li, S.: A general cooling trend on the central Tibetan Plateau
968 throughout the Holocene recorded by the lake Zigetang pollen spectra, *Quatern. Int.*, 154, 113-121,
969 doi:10.1016/j.quaint.2006.02.005, 2006b.
- 970
971 Herzsuh, U., Kramer A., Mischke S., and Zhang C.: Quantitative climate and vegetation trends since the late glacial
972 on the northeastern Tibetan Plateau deduced from Koucha lake pollen spectra, *Quaternary Res.*, 71, 162-171,
973 doi:10.1016/j.yqres.2008.09.003, 2009.
- 974 Hillenbrand, C.-D., and Fütterer, D.K.: Neogene to Quaternary deposition of opal on the continental rise west of the
975 Antarctic Peninsula, ODP Leg 178, Sites 1095, 1096, and 1101. In: Barker, P.F., Camerlenghi, A., Acton, G.D.,
976 Ramsay, A.T.S. (Eds.), *Proceedings of the Ocean Drilling Programme, Scientific Results*, 178. Texas A and M Uni-
977 versity, College Station, Texas, pp. 1–40 (CD-ROM), 2002.
- 978 Hillyer, R., Valencia, B. G., Bush, M.B., Silman, M.R., and Steinitz-Kannan, M.: A 24,700-yr paleolimnological history
979 from the Peruvian Andes, *Quaternary Res.*, 71, 71-82, doi:10.1016/j.yqres.2008.06.006, 2009.
- 980 Hobley, D.E., Sinclair, H.D., and Cowie, P.A.: Processes, rates, and time scales of fluvial response in an ancient postglacial
981 landscape of the northwest Indian Himalaya. *Geological Society of America Bulletin*, 122, 1569-1584, 2010.
- 982 Hodell, D. A., Brenner, M., Kanfoush, S. L., Curtis, J. H., Stoner, J. S., Song, X., Wu, Y., and Whitmore, T. J.: Paleocli-
983 mate of southwestern China for the past 50,000 yr inferred from lake sediment records, *Quaternary Res.*, 52, 369-
984 380, doi:10.1006/qres.1999.2072, 1999.
- 985 Hu, G., Yi, C.-L., Zhang, J.-F., Liu, J.-L., Jiang, T., and Qin, X.: Optically stimulated luminescence dating of a moraine
986 and a terrace in Laohugou valley, western Qilian Shan, northeastern Tibet, *Quaternary International* 321, 37-49,
987 doi:10.1016/j.quaint.2013.12.019, 2014.
- 988 Insel, N., Poulsen, C.J., and Ehlers, T.A.: Influence of the Andes Mountains on South American moisture transport, con-
989 vection, and precipitation, *Climate Dynamics*, 35 (7-8), 1477-1492, 2010.
- 990 Jeffery, M.L., Ehlers, T.A., Yanites, B.J., and Poulsen, C.J.: Quantifying the role of paleoclimate and Andean Plateau
991 uplift on river incision: PALEOCLIMATE ROLE IN RIVER INCISION, *Journal of Geophysical Research: Earth*
992 *Surface*, 118(2), 852–871, doi:10.1002/jgrf.20055, 2013.
- 993 Jenny, B., Valero-Garcés, B. L., Urrutia, R., Kelts, K., Veit, H., and Geyh, M.: Moisture changes and fluctuations of the
994 Westerlies in Mediterranean Central Chile during the last 2000 years: The Laguna Aculeo record (33°50' S), *Quatern.*
995 *Int.*, 87, 3-18, doi:10.1016/S1040-6182(01)00058-1, 2002a.
- 996 Jenny, B., Valero-Garcés, B.L., Villa-Martínez, R., Urrutia, R., Geyh, M. A., and Veit, H.: Early to Mid-Holocene Arid-
997 ity in Central Chile and the Southern Westerlies: The Laguna Aculeo Record (34°S), *Quaternary Res.*, 58, 160–170,
998 doi:10.1006/qres.2002.2370, 2002b.

- 999 Jungclauss, J. H., Lorenz, S. J., Timmreck, C., Reick, C. H., Brovkin, V., Six, K., Segsneider, J., Giorgetta, M.A.,
1000 Crowley, T.J., Pongratz, J., Krivova, N.A., Vieira, L.E., Solanski, S.K., Klocke, D., Botzet, M., Esch, M., Gayler, V.,
1001 Haak, H., Raddatz, T.J., Roeckner, E., Schnur, R., Widmann, H., Claussen, M., Stevens, B., and Marotzke, J.:
1002 Climate and carbon-cycle variability over the last millennium. *Climate of the Past*, 6, 723-737. doi:10.5194/cp-6-723-
1003 2010, 2010.
- 1004 Junginger, A., Roller, S., Olaka, L. A., and Trauth, M. H.: The effects of solar irradiation changes on the migration of the
1005 Congo Air Boundary and water levels of paleo-Lake Suguta, Northern Kenya Rift, during the African Humid Period
1006 (15–5 ka BP), *Palaeogeogr. Palaeoclimatol.*, 396, 1-16, doi:10.1016/j.palaeo.2013.12.007, 2014.
- 1007 Kaiser, J., Schefuss, E., Lamy, F., Mohtadi, M., and Hebbeln, D.: Glacial to Holocene changes in sea surface temperat-
1008 ure and coastal vegetation in north central Chile : high *versus* low latitude forcing, *Quaternary Sci. Rev.*, 27, 2064–
1009 2075, doi:10.1016/j.quascirev.2008.08.025, 2008.
- 1010 Kalnay, E., Kanamitsu, M., Kistler, R., Collins, W., Deaven, D., Gandin, L., Iredell, M., Saha, S., White, G., Woollen, J.,
1011 Zhu, Y., Chelliah, M., Ebisuzaki, W., Higgins, W., Janowiak, J., Mo, K.C., Ropelewski, C., Wang, J., Leetmaa, A.,
1012 Reynolds, R., Jenne, R., and Joseph, D.: The NCEP/NCAR 40-year reanalysis project. *Bulletin of the American*
1013 *Meteorological Society*, 77(3), 437-471, 1996.
- 1014 Kashiwaya, K., Masuzawa, T., Morinaga, H., Yaskawa, K., Yuan, B. Y., Liu, J. Q., and Gu, Z.: Changes in hydrological
1015 conditions in the central Qing-Zang (Tibetan) Plateau inferred from lake bottom sediments, *Earth Planet. Sc. Lett.*,
1016 135, 31-39, doi:10.1016/0012-821X(95)00136-Z, 1995.
- 1017 Kent-Corson, M., Sherman, L., Mulch, A. and Chamberlain, C.: Cenozoic topographic and climatic response to chan-
1018 ging tectonic boundary conditions in Western North America, *Earth Planet. Sc. Lett.*, 252(3-4), 453-466,
1019 doi:10.1016/j.epsl.2006.09.049, 2006.
- 1020 Kistler, R., Collins, W., Saha, S., White, G., Woollen, J., Kalnay, E., Chelliah, M., Ebisuzaki, W., Kanamitsu, M.,
1021 Kousky, V., Van den Dool, H., Jenne, R., and Fiorino, M.: The NCEP–NCAR 50–Year Reanalysis: Monthly Means
1022 CD–ROM and Documentation. *Bulletin of the American Meteorological Society*, 82(2), 247–267, 2001.
- 1023 Kirchner, J.W., Finkel, R.C., Riebe, C.S., Granger, D.E., Clayton, J.L., King, J.G., and Megahan, W.F.: Mountain
1024 erosion over 10 yr, 10 k.y., and 10 m.y. time scales, *Geology*, 29 (7), 591-594, 2001.
- 1025 Knorr, G., Butzin, M., Micheels, A., and Lohmann, G.: A Warm Miocene Climate at Low Atmospheric CO2 levels.
1026 *Geophysical Research Letters*, 38, L20701, doi:10.1029/2011GL048873, 2011.
- 1027 Koons, P.O., Zeitler, P.K., and Hallet, B.: 5.14 Tectonic Aneurysms and Mountain Building, in *Treatise on Geomorpho-*
1028 *logy*, pp. 318–349, Elsevier, 2013.
- 1029 Kotlia, B. S., Sharma, C., Bhalla, M. S., Rajagopalan, G., Subrahmanyam, K., Bhattacharya, A., and Valdiya, K. S.: Pa-
1030 leoclimatic conditions in the late Pleistocene Wadda Lake, eastern Kumaun Himalaya (India), *Palaeogeogr. Pa-*
1031 *laeoclimatol.*, 162, 105-118, doi:10.1016/S0031-0182(00)00107-3, 2000.
- 1032 Kramer, A., Herzschuh, U., Mischke, S., and Zhang, C.: Late glacial vegetation and climate oscillations on the south-
1033 eastern Tibetan Plateau inferred from the lake Naleng pollen profile, *Quaternary Res.*, 73, 324-335,

- 1034 doi:10.1016/j.yqres.2009.12.003, 2010.
- 1035 Kraus, H.: Die Atmosphäre der Erde. Eine Einführung in die Meteorologie. Berlin, 2001.
- 1036 Kutzbach, J.E., Guetter, P.J., Ruddiman, W.F., and Prell, W.L.: Sensitivity of Climate to Late Cenozoic Uplift in
1037 Southern Asia and the American West - Numerical Experiments, *Journal of Geophysical Research-Atmospheres*,
1038 94(D15), 18393-18407, 1989.
- 1039 Kutzbach, J.E., Prell, W.L., and Ruddiman, W.F.: Sensitivity of Eurasian Climate to Surface Uplift of the Tibetan Plat-
1040 eau, *Journal of Geology*, 101(2), 177-190, 1993.
- 1041 Lamy, F. and Kaiser, J.: Past Climate Variability in South America and Surrounding Regions, Chapter 6: Glacial to
1042 Holocene Paleoceanographic and Continental Paleoclimate Reconstructions Based on ODP Site 1233/GeoB 3313
1043 Off southern Chile, 2009.
- 1044 Lamy, F., Hebbeln, D., and Wefer, G.: High Resolution Marine Record of Climatic Change in Mid-latitude Chile during
1045 the Last 28,000 Years Based on Terrigenous Sediment Parameters, *Quaternary Res.*, 51, 83-93,
1046 doi:10.1006/qres.1998.2010, 1999.
- 1047 Lamy, F., Klump, J., Hebbeln, D., and Wefer, G.: Late Quaternary rapid climate change in northern Chile, *Terra Nova*,
1048 12, 8-13, doi:10.1046/j.1365-3121.2000.00265.x, 2000.
- 1049 Lamy, F., Rühlemann, C., Hebbeln, D. and Wefer, G.: High- and low-latitude climate control on the position of the
1050 southern Peru-Chile Current during the Holocene, *Paleoceanography*, 17, 16-1–16-10, doi:10.1029/2001PA000727,
1051 2002.
- 1052 Latorre, C., Betancourt, J., Rylander, K., and Quade, J.: Vegetation invasions into absolute desert: A 45 000 yr rodent
1053 midden record from the Calama-Salar de Atacama basins, northern Chile (lat 22° - 24°S), *Geol. Soc. Am. Bull.*, 114,
1054 349–366, doi:10.1130/0016-7606(2002)114<0349:VIIADA>2.0.CO;2, 2002.
- 1055 Latorre, C., Betancourt, J.L., Rylander, K.A., Quade, J., and Matthei, O.: A vegetation history from the arid prepuna of
1056 northern Chile (22-23°S) over the last 13500 years, *Palaeogeogr. Palaeocl.*, 194, 223-246, doi:10.1016/S0031-
1057 0182(03)00279-7, 2003.
- 1058 Latorre, C., Betancourt, J.L., and Arroyo, M.T.K.: Late Quaternary vegetation and climate history of a perennial river
1059 canyon in the Río Salado basin (22°S) of northern Chile, *Quaternary Res.*, 65, 450-466,
1060 doi:10.1016/j.yqres.2006.02.002, 2006.
- 1061 Lechler, A. and Niemi, N.: Sedimentologic and isotopic constraints on the Paleogene paleogeography and
1062 paleotopography of the southern Sierra Nevada, California, *Geology*, 39(4), 379-382, doi:10.1130/g31535.1, 2011.
- 1063 Lechler, A., Niemi, N., Hren, M. and Lohmann, K.: Paleoelevation estimates for the northern and central proto-Basin
1064 and Range from carbonate clumped isotope thermometry, *Tectonics*, 32(3), 295-316, doi:10.1002/tect.20016, 2013.
- 1065 Lease, R.O., and Ehlers, T.A.: Incision into the Eastern Andean Plateau During Pliocene Cooling, *Science*, 341(6147),
1066 774–776, doi:10.1126/science.1239132, 2013.
- 1067 Legates, D.R., and Willmott, C.J.: Mean Seasonal and Spatial Variability in Gauge-Corrected, Global Precipitation, *In-
1068 ternational Journal of Climatology* 10(2), 111-127. doi: 10.1002/joc.3370100202, 1990.
- 1069 Li, J., Ehlers, T.A., Werner, M., Mutz, S.G., Steger, C., Paeth, H.: Late quaternary climate, precipitation $\delta^{18}\text{O}$, and In-

- 1070 dian monsoon variations over the Tibetan Plateau. *Earth and Planetary Science Letters* 457, 412-422, 2017.
- 1071 Liu, X., Colman, S. M., Brown, E. T., An, Z., Zhou, W., Jull, A. J. T., Huang, Cheng, Y., P., Liu, W., and Xu, H.: A
1072 climate threshold at the eastern edge of the Tibetan plateau, *Geophys. Res. Lett.*, doi: 10.1002/2014GL060833,
1073 2014.
- 1074 Licht, A., Quade, J., Kowler, A., de los Santos, M., Hudson, A., Schauer, A., Huntington, K., Copeland, P. and Lawton,
1075 T.: Impact of the North American monsoon on isotope paleoaltimeters: Implications for the paleoaltimetry of the
1076 American southwest, *Am. J. Sci.*, 317(1), 1-33, doi:10.2475/01.2017.01, 2017.
- 1077 Lohmann, G., Pfeiffer, M., Laepple, T., Leduc, G., and Kim, J.-H.: A model-data comparison of the Holocene global sea
1078 surface temperature evolution. *Clim. Past*, 9, 1807-1839, doi:10.5194/cp-9-1807-2013, 2013.
- 1079
- 1080 Lorenz, S.J., and Lohmann, G.: Acceleration technique for Milankovitch type forcing in a coupled atmosphere-ocean
1081 circulation model: method and application for the Holocene. *Climate Dynamics* (2004) 23: 727.
1082 doi:10.1007/s00382-004-0469-y, 2004.
- 1083
- 1084 Maldonado, A. and Villagrán, C.: Climate variability over the last 9900 cal yr BP from a swamp forest pollen record
1085 along the semiardi coast of Chile, *Quaternary Res.*, 66, 146-258, doi:10.1016/j.yqres.2006.04.003, 2006.
- 1086 Maldonado, A. J., Betancourt, J. L., Latorre, C., and Villagrán, C.: Pollen analyses from a 50000-yr rodent midden
1087 series in the southern Atacama Desert (25°30' S), *J. Quaternary Sci.*, 20, 493-507, doi:10.1002/jqs.936, 2005.
- 1088 Maldonado, A., Méndez, C., Ugalde, P., Jackson, D., Seguel, R., and Latorre, C.: Early Holocene climate change and
1089 human occupation along the semiarid coast of north-central Chile, *J. Quaternary Sci.*, 25, 985-988,
1090 doi:10.1002/jqs.1385, 2010.
- 1091 Markgraf, V., Bradbury, J. P., Schwalb, A., Burns, S., Stern, C., Ariztegui, D., Gilli, D., Anselmetti, F. S., Stine, S., and
1092 Maidana, N.: Holocene palaeoclimates of southern Patagonia: limnological and environmental history of Lago
1093 Cardiel, Argentina, *Holocene*, 13, 581-591, doi:10.1191/0959683603hl648rp, 2003.
- 1094 Markgraf, V., Whitlock, C., and Haberle, S.: Vegetation and fire history during the last 18,000 cal yr B.P. in Southern
1095 Patagonia: Mallín Pollux, Coyhaique, Province Aisén (45°41'30" S, 71°50'30" W, 640 m elevation), *Palaeogeogr.*
1096 *Palaeocl.*, 254, 492-507, doi:10.1016/j.palaeo.2007.07.008, 2007.
- 1097 Maroon, E. A., Frierson, D. M. W., and Battisti, D. S.: The tropical precipitation response to Andes topography and
1098 ocean heat fluxes in an aquaplanet model, *J. Climate*, 28, 381-398, doi:10.1175/JCLI-D-14-00188.1, 2015.
- 1099 Maroon, E. A., Frierson, D. M. W., Kang, S. M., and Scheff, J.: The precipitation response to an idealized subtropical
1100 continent, *J. Climate*, 29, 4543-4564, doi:10.1175/JCLI-D-15-0616.1, 2016.
- 1101 Marshall, J.A., Roering, J.J., Bartlein, P.J., Gavin, D.G., Granger, D.E., Rempel, A.W., Praskievicz, S.J., and Hales,
1102 T.C.: Frost for the trees: Did climate increase erosion in unglaciated landscapes during the late Pleistocene? *Science*
1103 *Advances*, 1, 1-10, 2015.
- 1104 Marston, R.A.: Geomorphology and vegetation on hillslopes: Interactions, dependencies, and feedback loops, *Geomor-*
1105 *phology*, 116(3-4), 206-217. doi:http://doi.org/10.1016/j.geomorph.2009.09.028, 2010.
- 1106 Matsuoka, N., and Murton, J.: Frost weathering: Recent advances and future directions. *Permafrost Periglacial Process.* 19,
1107 195-210, 2008.
- 1108 Matsuoka, N.: Solifluction rates, processes and landforms: A global review. *Earth Science Reviews* 55, 107-134, 2001.

- 1109 Maussion, F., Scherer, D., Mölg, T., Collier, E., Curio, J., and Finkelnburg, R.: Precipitation seasonality and variability
1110 over the Tibetan Plateau as resolved by the High Asia Reanalysis, *J. Climate*, 27, 1910-1927, doi:10.1175/JCLI-D-
1111 13-00282.1, 2014
- 1112 Méndez, C., Gil, A., Neme, G., Nuevo Delaunay, A., Cortegoso, V., Huidobro, C., Durán, and Maldano, A.: Mid
1113 Holocene radiocarbon ages in the Subtropical Andes (~29° - 35° S), climatic change an implicaton for human space
1114 organization, *Quatern. Int.*, 356, 15-26, doi:10.1016/j.quaint.2014.06.059, 2015.
- 1115 Mesinger, F., DiMego, G., Kalnay, E., Mitchell, K., Shafran, P.C., Ebisuzaki, W., Jovic, D., Woollen, J., Rogers, E.,
1116 Berbery, E.H., Ek, M.B., Fan, Y., Grumbine, R., Higgins, W., Li, H., Lin, Y., Manikin, G., Parrish, D., and Shi,
1117 W.:North American Regional Reanalysis, *Bulletin of the American Meteorological Society*, 87, 343–
1118 360.doi:10.1175/BAMS-87-3-343, 2006.
- 1119 Methner, K., Fiebig, J., Wacker, U., Umhoefer, P., Chamberlain, C. and Mulch, A.: Eocene-Oligocene proto-Cascades
1120 topography revealed by clumped ($\Delta 47$) and oxygen isotope ($\delta 18O$) geochemistry (Chumstick Basin, WA, USA),
1121 *Tectonics*, 35(3), 546-564, doi:10.1002/2015tc003984, 2016.
- 1122 Mischke S., Kramer M., Herzsuh U., Shang H., Erzinger J., and Zhang C.: Reduced early holocene moisture
1123 availability in the Bayan Har Mountains, northeastern Tibetan Plateau, inferred from a multi-proxy lake record,
1124 *Palaeogeogr. Palaeocl*, 267, 59-76, doi:10.1016/j.palaeo.2008.06.002, 2008.
- 1125 Molnar, P., Boos, W.R., and Battisti, D.S.: Orographic Controls on Climate and Paleoclimate of Asia: Thermal and
1126 Mechanical Roles for the Tibetan Plateau, *Annual Review of Earth and Planetary Sciences*, 38, 77-102, 2010.
- 1127 Molnar, P., and England, P.: Late Cenozoic uplift of mountain ranges and global climate change: chicken or egg?,
1128 *Nature*, 346, 29-34, 1990.
- 1129 Montgomery, D.R.: Slope distributions, threshold hillslopes, and steady-state topography, *American Journal of Science*,
1130 301, 432-454, 2001.
- 1131 Montgomery, D.R., Balco, G., and Willett, S.D.: Climate, tectonics, and the morphology of the Andes, *Geology*, 29(7),
1132 579-582, 2001.
- 1133 Moon, S., Chamberlain, C.P., Blisniuk, K., Levine, N., Rood, D.H., Hilley, G.E.: Climatic control of denudation in the
1134 deglaciaded landscape of the Washington Cascades, *Nature Geoscience*, 4, 469-473, 2011.
- 1135 Moreno, A., Santoro, C. M., and Latorre, C.: Climate change and human occupation in the northernmost Chilean
1136 Altiplano over the last ca. 11500 cal. a BP, *Quaternary Sci.*, 24, 373–382, doi:10.1002/jqs.1240, 2009.
- 1137 Morinaga, H., Itota, C., Isezaki, N., Goto, H., Yaskawa, K., Kusakabe, M., Liu, J., Gu, Z., Yuan, B., and Cong, S.:
1138 Oxygen-18 and carbon-13 records for the last 14,000 years from lacustrine carbonates of Siling-Co (lake) in the
1139 Qinghai-Tibetan Plateau, *Geophys. Res. Lett.*, 20, 2909-2912, doi:10.1029/93GL02982, 1993.
- 1140 Morrill, C., Overpeck, J. T., Cole, J. E., Liu, K., Shen, C., and Tang, L.: Holocene variations in theAsian monsoon in-
1141 ferred from the geochemistry of lake sediments in central Tibet, *Quaternary Res.*, 65, 232-243,
1142 doi:10.1016/j.yqres.2005.02.014, 2006.
- 1143 Moulton, K.L., and Berner, R.A.: Quantification of the effect of plants on weathering: studies in Iceland, *Geology*, 26,

- 1144 895-898, 1998.
- 1145 Muegler, I., Gleixner, G., Guenther, F., Maeusbacher, R., Daut, G., Schuett, B., Berking, J., Schwalb, A., Schwark, L.,
1146 Xu, B., Yao, T., Zhu, L., and Yi, C.: A multi-proxy approach to reconstruct hydrological changes and Holocene
1147 climate development of Nam Co, Central Tibet, *J. Paleolimnol.*, 43, 625-648, doi:10.1007/s10933-009-9357-0, 2010.
- 1148 Mujica, M. I., Latorre, C., Maldonado, A., González-Silvestre, L., Pinto, R., De Pol-Holz, R., and Santoro, C. M.: Late
1149 Quaternary climate change, relict populations and present-day refugia in the northern Atacama Desert: a case study
1150 from Quebrada La Higuera (18° S), *J. Biogeogr.*, 42, 76–88, doi:10.1111/jbi.12383, 2015.
- 1151 Mulch, A., Sarna-Wojcicki, A., Perkins, M. and Chamberlain, C.: A Miocene to Pleistocene climate and elevation record
1152 of the Sierra Nevada (California), *P. Natl. Acad. Sci. USA*, 105(19), 6819-6824, doi:10.1073/pnas.0708811105,
1153 2008.
- 1154
1155 Mulch, A., Chamberlain, C., Cosca, M., Teyssier, C., Methner, K., Hren, M. and Graham, S.: Rapid change in high-elev-
1156 ation precipitation patterns of western North America during the Middle Eocene Climatic Optimum (MECO), *Am. J.*
1157 *Scie.*, 315(4), 317-336, doi:10.2475/04.2015.02, 2015.
- 1158 Mutz, S.G., Ehlers, T.A., Li, J., Steger, C., Peath, H., Werner, M., Poulsen, C.J.: Precipitation $\delta^{18}\text{O}$ over the South Asia
1159 Orogen from ECHAM5-wiso Simulation: Statistical Analysis of Temperature, Topography and Precipitation.
1160 *Journal of Geophysical Research-Atmospheres*, 121(16),9278-9300, doi: 10.1002/2016JD024856, 2016.
- 1161 Nishimura, M., Matsunaka, T., Morita, Y., Watanabe, T., Nakamura, T., Zhu, L., Nara, W. F., Imai, A., Izutsu, Y., and
1162 Hasuike, N.: Paleoclimatic changes on the southern Tibetan Plateau over the past 19,000 years recorded in lake
1163 Pumoyum Co, and their implications for the southwest monsoon evolution, *Palaeogeogr. Palaeocl.*, 396, 75-92,
1164 doi:10.1016/j.palaeo.2013.12.015, 2014.
- 1165 Otto-Bliesner, B.L., Brady, C.B., Clauzet, G., Tomas, R., Levis, S., and Kothavala, Z.: Last Glacial Maximum and
1166 Holocene Climate in CCSM3. *Journal of Climate*, 19, 2526-2544, 2006.
- 1167 Paeth, H.: Key Factors in African Climate Change Evaluated by a Regional Climate Model, *Erdkunde*, 58, 290-315,
1168 2004.
- 1169 Peel, M.C., Finlayson, B.L., McMahon, T.A.: Updated world map of the Koppen- Geiger climate classification.
1170 *Hydro. Earth Syst. Sci.* 11, 1633–1644, 2007.
- 1171
1172 Pfeiffer, M., and Lohmann, G.: Greenland Ice Sheet influence on Last Interglacial climate: global sensitivity studies
1173 performed with an atmosphere-ocean general circulation model. *Climate of the Past*, 12, pp. 1313-1338,
1174 doi:10.5194/cp-12-1313-2016, 2016.
- 1175 Pickett, E.J., Harrison, S.P., Flenley, J., Grindrod, J., Haberle, S., Hassell, C., Kenyon, C., MacPhail, M., Martin, H.,
1176 Martin, A.H., McKenzie, M., Newsome, J.C., Penny, D., Powell, J., Raine, J.I., Southern, W., Stevenson, J., Sutra,
1177 J.-P., Thomas, I., van der Kaars, S., Ward, J.: Pollen-based reconstructions of biome distributions for Australia,
1178 South-East Asia and the Pacific (SEAPAC region) at 0, 6000 and 18,000 14C years B.P.. *Journal of Biogeography*,
1179 31, 1381–1444, doi: 10.1111/j.1365-2699.2004.01001.x, 2004.
- 1180
1181 Pingel, H., Mulch, A., Alonso, R., Cottle, J., Hynek, S., Poletti, J., Rohrmann, A., Schmitt, A., Stockli, D. and Strecker,
1182 M.: Surface uplift and convective rainfall along the southern Central Andes (Angastaco Basin, NW Argentina),
1183 *Earth Planet. Sc. Lett.*, 440, 33-42, doi:10.1016/j.epsl.2016.02.009, 2016.

1184
1185 Prentice, I. C., Jolly, D., and BIOME 6000 Participants. (2000). Mid-Holocene and glacial-maximum vegetation geo-
1186 graphy of the northern continents and Africa. *Journal of Biogeography* 27, 507-519.
1187
1188 Pueyo, J. J., Sáez, A., Giralt, S., Valero-Garcés, B.L., Moreno, A., Bao, R., Schwalb, A., Herrera, C., Klosowska, B.,
1189 and Taberner, C.: Carbonate and organic matter sedimentation and isotopic signatures in Lake Chungará, Chilean
1190 Altiplano, during the last 12.3 kyr, *Palaeogeogr. Palaeocl.*, 307, 339-355, doi:10.1016/j.palaeo.2011.05.036, 2011.

1191 Quade, J., Rech, J. A., Betancourt, J. L., Latorre, C., Quade, B., Rylander, K. A., and Fisher, T.: Paleowetlands and re-
1192 gional climate change in the central Atacama Desert, northern Chile, *Quaternary Res.*, 69, 343-360,
1193 doi:10.1016/j.yqres.2008.01.003, 2008.

1194 Raymo, M.E., and Ruddiman, W.F.: Tectonic forcing of late cenozoic climate. *Nature*, 359(6391), 117-122, 1992.

1195 Rech, J. A., Pigati, J. S., Quade, J., and Betancourt, J. L.: Re-evaluation of mid-Holocene deposits at Quebrada Puripica,
1196 northern Chile, *Palaeogeogr. Palaeocl.*, 194, 207-222, doi:0.1016/S0031-0182(03)00278-5, 2003.

1197 Robinson, M.M.: New quantitative evidence of extreme warmth in the Pliocene Arctic, *Stratigraphy* 6, 265–275, 2009.

1198 Roeckner, E., Bäuml, G., Bonaventura, L., Brokopf, R., Esch, M., Giorgetta, M., Hagemann, S., Kirchner, I., Korn-
1199 blueh, L., Manzini, E., Rhodin, A., Schlese, U., Schulzweida, U., and Tompkins, A.: The atmospheric general circu-
1200 lation model ECHAM5. Part I: Model description. Rep. 349Rep., 127 pp, Max Planck Institute for Meteorology,
1201 Hamburg, 2003.

1202 Roering, J.J., Marshall, J., Booth, A.M., Mort, M., and Jin, Q.: Evidence for biotic controls on topography and soil pro-
1203 duction, *Earth and Planetary Science Letters*, 298(1–2), 183–190, doi:10.1016/j.epsl.2010.07.040, 2010.

1204 Salzmann, U., Williams, M., Haywood, A.M., Johnson, A.L.A., Kender, S., and Zalasiewicz, J.: Climate and environ-
1205 ment of a Pliocene warm world. *Palaeogeography, Palaeoclimatology, Palaeoecology*, 309 (1-8), 2011.

1206 Sarnthein, M.: Sand deserts during glacial maximum and climatic optimum, *Nature*, 272, 43–46, doi:10.1038/272043a0,
1207 1978.

1208 Sarnthein, M., Gersonde, R., Niebler, S., Pflaumann, U., Spielhagen, R., Thiede, J., Wefer, G., Weinelt, M.: Overview of
1209 Glacial Atlantic Ocean Mapping (GLAMAP 2000), *Paleoceanography*, 18(2), doi:10.1029/2002PA000769, 2003.

1210 Schäfer-Neth C., and Paul, A.: The Atlantic Ocean at the last glacial maximum: objective mapping of the GLAMAP
1211 sea-surface conditions. In: Wefer G, Mulitza S, Rasmussen V (eds) *The South Atlantic in the late quaternary: recon-*
1212 *struction of material budgets and current systems.* Springer, Berlin, pp 531–548, 2003.

1213 Schaller, M., von Blanckenburg, F., Veldkamp, A., Tebbens, L.A., Hovius, N., and Kubik, P.W.: A 30 000 yr record of
1214 erosion rates from cosmogenic ¹⁰Be in Middle European river terraces, *Earth and Planetary Science Letters*,
1215 204(1), 307–320, 2002.

1216 Schaller, M., and Ehlers T.A.: Limits to quantifying climate driven changes in denudation rates with cosmogenic radio-
1217 nuclides, *Earth and Planetary Science Letters*, v. 248, pp. 153-167. doi:10.1016/j.epsl.2006.05.027, 2006.

- 1218 Schwalb, A., Burns, S., and Kelts, K.: Holocene environments from stable isotope stratigraphy of ostracods and authi-
1219 genic carbonate in Chilean Altiplano Lakes, *Palaeogeogr. Palaeoclimatol.*, 148, 153-168, doi:10.1016/S0031-
1220 0182(98)00181-3, 1999.
- 1221 Shen J., Liu X. Q., Wang S. M., and Matsumoto R.: Palaeoclimatic changes in the Qinghai, Lake area during the last
1222 18,000 years, *Quatern. Int.*, 136, 131-140, doi:10.1016/j.quaint.2004.11.014, 2005.
- 1223 Shen C., Liu K., Tang L., and Overpeck J. T.: Quantitative relationships between modern pollen rain and climate in the
1224 Tibetan Plateau. *Rev. Palaeobot. Palynol.*, 140, 61–77, doi:10.1016/j.revpalbo.2006.03.001, 2006.
- 1225 Siani, G., Colin, C., Michel, E., Carel, M., Richter, T., Kissel, C., and Dewilde, F.: Late Glacial to Holocene terrigenous
1226 sediment record in the Northern Patagonian margin: Paleoclimate implications, *Palaeogeogr. Palaeoclimatol.*, 297, 26-36,
1227 doi:10.1016/j.palaeo.2010.07.011, 2010.
- 1228 Simmons, A.J., Burridge, D.M., Jarraud, M., Girard, C., and Wergen, W.: The ECMWF Medium-Range prediction mod-
1229 els development of the numerical formulations and the impact of increased resolution, *Meteorology and Atmo-
1230 spheric Physics*, 40(1-3), 28-60, 1989.
- 1231 Sohl, L.E., Chandler, M.A., Schmunk, R.B., Mankoff, K., Jonas, J.A., Foley, K.M., and Dowsett, H.J.: PRISM3/GISS
1232 topographic reconstruction, *U.S. Geological Survey Data Series*, 419, 6p., 2009.
- 1233
- 1234 Sowers T., Alley, R.B., and Jubenville, J.: Ice core records of atmospheric N₂O covering the last 106,000 years. *Science*,
1235 301:945–948, 2003.
- 1236
- 1237 Stepanek, C., and Lohmann, G.: Modelling mid-Pliocene climate with COSMOS , *Geosci. Model Dev.* , 5 , pp. 1221-
1238 1243 . doi:10.5194/gmd-5-1221-2012, 2012.
- 1239 Stine, S. and Stine M.: A record from Lake Cardiel of climate change in southern South America, *Nature*, 345, 705-708,
1240 doi:10.1038/345705a0,1990.
- 1241 Szeicz, J. M., Haberle, S. G., and Bennett, K. D.: Dynamics of North Patagonian rainforests from fine-resolution pollen,
1242 charcoal and tree-ring analysis, Chonos Archipelago, Southern Chile, *Austral Ecol.*, 28, 413–422,
1243 doi:10.1046/j.1442-9993.2003.01299.x , 2003.
- 1244 Takahashi, K., and Battisti, D.: Processes controlling the mean tropical pacific precipitation pattern. Part I: The Andes
1245 and the eastern Pacific ITCZ. *Journal of Climate*, 20(14), 3434-3451, 2007a.
- 1246 Takahashi, K., and Battisti, D.: Processes controlling the mean tropical pacific precipitation pattern. Part II: The SPCZ
1247 and the southeast pacific dry zone. *Journal of Climate*, 20(23), 5696-5706, 2007b.
- 1248 Tang, L., Shen, S., Liu, K., and Overpeck, J. T.: Changes in south Asian monsoon: new high-resolution paleoclimatic re-
1249 cords from Tibet, China, *Chinese Sci. Bull.*, 45, 87-91, doi:10.1007/BF02884911, 2000.
- 1250 Thiede, R.C., and Ehlers, T.A.: Large spatial and temporal variations in Himalayan denudation. *Earth and Planetary
1251 Science Letters*, 374, 256-257. doi:10.1016/j.epsl.2013.03.004, 2013.

- 1252 Thomas, A.: The climate of the Gongga Shan range, Sichuan Province, PR China. *Arctic and Alpine Research*, 29(2),
1253 226-232, 1997.
- 1254 Uppala, S.M., Kállberg, P.W., Simmons, A.J., Andrae, U., da Costa Bechtold, V., Fiorino, M., Gibson, J.K., Haseler, J.,
1255 Hernandez, A., Kelly, G.A., Li, X., Onogi, K., Saarinen, S., Sokka, N., Allan, R.P., Andersson, E., Arpe, K.,
1256 Balmaseda, M.A., Beljaars, A.C.M., van de Berg, L., Bidlot, J., Bormann, N., Caires, S., Chevallier, F., Dethof, A.,
1257 Dragosavac, M., Fisher, M., Fuentes, M., Hagemann, S., Hólm, E., Hoskins, B.J., Isaksen, I., Janssen, P.A.E.M.,
1258 Jenne, R., McNally, A.P., Mahfouf, J.-F., Morcrette, J.-J., Rayner, N.A., Saunders, R.W., Simon, P., Sterl, A.,
1259 Trenberth, K.E., Untch, A., Vasiljevic, D., Viterbo, P., and Woollen, J.: The ERA-40 re-analysis. *Quart. J. R.*
1260 *Meteorol. Soc.*, 131, 2961-3012, 2005.
- 1261
- 1262 von Blanckenburg, F., Bouchez, J., Ibarra, D.E., and Maher, K.: Stable runoff and weathering fluxes into the oceans
1263 over Quaternary climate cycles, *Nature Geoscience*, 8(7), 538–542, doi:10.1038/ngeo2452, 2015.
- 1264 Valla, P.G., Shuster, D.L., and van der Beek, P.A.: Significance increase in relief of European Alps during mid-Pleisto-
1265 cene glaciations. *Nature Geoscience*, 4, 688–692. doi:10.1038/ngeo1242, 2011.
- 1266 Van Campo, E., Cour, P., and Huang, S.: Holocene environmental changes in Bangong Co basin (Western Tibet). Part 2:
1267 The pollen record, *Palaeogeogr. Palaeoclimatol.*, 120, 49-63, doi:10.1016/0031-0182(95)00033-X, 1996.
- 1268
- 1269 Villagrán, C. and Varela, J.: Palynological Evidence for Increased Aridity on the Central Chilean Coast during the
1270 Holocene, *Quaternary Res.*, 34, 198–207, doi:10.1016/0033-5894(90)90031-F, 1990.
- 1271 Villa-Martínez, R., Villagrán, C., and Jenny, B.: The last 7500 cal yr B.P. of westerly rainfall in Central Chile inferred
1272 from a high-resolution pollen record from Laguna Aculeo (34°S), *Quaternary Res.*, 60, 284-293,
1273 doi:https://doi.org/10.1016/j.yqres.2003.07.007, 2003.
- 1274 Wei, W., and Lohmann, G.: Simulated Atlantic Multidecadal Oscillation during the Holocene. *Journal of Climate*, 25,
1275 6989–7002. doi: http://dx.doi.org/10.1175/JCLI-D-11-00667.1, 2012.
- 1276 Wang, R.L., Scarpitta, S. C., Zhang, S. C., and Zheng, M. P.: Later Pleistocene/Holocene climate conditions of Qinghai-
1277 Xizhang Plateau (Tibet) based on carbon and oxygen stable isotopes of Zabuye Lake sediments, *Earth Planet. Sc.*
1278 *Letts.*, 203, 461-477, doi:10.1016/S0012-821X(02)00829-4, 2002.
- 1279 Whipple, K.X., Kirby, E., and Broecklehurst, S.H.: Geomorphic limits to climate-induced increases in topographic re-
1280 lief. *Nature*, 401, 39-43. doi:10.1038/43375, 1999.
- 1281 Whipple, K.X., and Tucker, G.E.: Dynamics of the stream-power river incision model: Implications for height limits of
1282 mountain ranges, landscape response timescales, and research needs, *Journal of Geophysical Research-Solid Earth*,
1283 104, 17661-17674, 1999.
- 1284 Whipple, K. X.: The influence of climate on the tectonic evolution of mountain belts, *Nat. Geosci.*, 2,
1285 doi:10.1038/ngeo413, 2009.
- 1286 Wilks, D.S.: *Statistical methods in the atmospheric sciences* - 3rd ed. Academic Press, Oxford, 2011.
- 1287 Willett, S.D., Schlunegger, F., and Picotti, V.: Messinian climate change and erosional destruction of the central

- 1288 European Alps. *Geology*, 34(8), 613-616, 2006.
- 1289 Wilson, G.S., Barron, J.A., Ashworth, A.C., Askin, R.A., Carter, J.A., Curren, M.G., Dalhuisen, D.H., Friedmann, E.I.,
1290 Fyodorov-Davidov, D.G., Gilichinsky, D.A., Harper, M.A., Harwood, D.M., Hiemstra, J.F., Janecek, T.R., Licht,
1291 K.J., Ostroumov, V.E., Powell, R.D., Rivkina, E.M., Rose, S.A., Stroeven, A.P., Stroeven, P., van der Meer, J.J.M.,
1292 Wizevich, M.C.: The Mount Feather Diamicton of the Sirius Group: an accumulation of indicators of Neogene Ant-
1293 arctic glacial and climatic history, *Palaeogeography, Palaeoclimatology, Palaeoecology*, 182 (1–2), 117–131, 2002.
- 1294 Wischniewski, J., Mischke, S., Wang, Y., and Herzschuh, U.: Reconstructing climate variability on the northeastern
1295 Tibetan Plateau since the last lateglacial – a multi-proxy, dual-site approach comparing terrestrial and aquatic
1296 signals, *Quaternary Science Reviews*, 30, 82-97, doi:10.1016/j.quascirev.2010.10.001, 2011.
- 1297 Wünnemann, B., Mischke, S., and Chen, F.: A Holocene sedimentary record from Bosten lake, China, *Palaeogeogr. Pa-*
1298 *laeocl.*, 234, 223-238, doi:10.1016/j.palaeo.2005.10.016, 2006.
- 1299 Yanhong, W., Lücke, A., Zhangdong, J., Sumin, W., Schleser, G.H., Battarbee, R.W., and Weilan, X.: Holocene climate
1300 development on the central Tibetan Plateau: A sedimentary record from Cuoe Lake, *Palaeogeogr. Palaeocl.*, 234,
1301 328-340, doi:10.1016/j.palaeo.2005.09.017, 2006
- 1302 Yanites, B.J., and Ehlers, T.A.: Global climate and tectonic controls on the denudation of glaciated mountains. *Earth*
1303 *and Planetary Science Letters*, 325, 63-75, 2012.
- 1304 Yu, L. and Lai, Z.: Holocene climate change inferred from stratigraphy and OSL chronology of Aeolian sediments in the
1305 Qaidam Basin, northeastern Qinghai-Tibetan Plateau, *Quaternary Res.*, 81, 488-499,
1306 doi:10.1016/j.yqres.2013.09.006, 2014.
- 1307 Zhang, C. and Mischke, S.: A lateglacial and Holocene lake record from the Nianbaoyeze Mountains and inferences of
1308 lake, glacier and climate evolution on the eastern Tibetan Plateau, *Quaternary Sci. Rev.*, 28, 1970-1983,
1309 doi:10.1016/j.quascirev.2009.03.007, 2009.
- 1310 Zhang, J., Chen, F., Holmes, J. A., Li, H., Guao, X., Wang, J., Li, S., Lu, Y., Zhao, Y., and Qiang, M.: Holocene mon-
1311 soon climate documented by oxygen and carbon isotopes from lake sediments and peat bogs in China: a review and
1312 synthesis, *Quaternary Sci. Rev.*, 30, 1973-1987, doi:10.1016/j.quascirev.2011.04.023, 2011.
- 1313 Zhang, X., Lohmann, G., Knorr, G., and Xu X.: Different ocean states and transient characteristics in Last Glacial Max-
1314 imum simulations and implications for deglaciation. *Clim. Past*, 9, 2319-2333, doi:10.5194/cp-9-2319-2013, 2013a.
- 1315 Zhang, R., Yan, Q., Zhang, Z.S., Jiang, D., Otto-Bliesner, B.L., Haywood, A.M., Hill, D.J., Dolan, A.M., Stepanek, C.,
1316 Lohmann, G., Contoux, C., Bragg, F., Chan, W.-L., Chandler, M.A., Jost, A., Kamae, Y., Abe-Ouchi, A., Ramstein,
1317 G., Rosenbloom, N.A., Sohl, L., and Ueda, H.: East Asian monsoon climate simulated in the PliomIP. *Clim. Past*, 9,
1318 2085-2099, doi:10.5194/cp-9-2085-2013, 2013b.
- 1319
- 1320 Zhang, X., Lohmann, G., Knorr, G., and Purcell C.: Abrupt glacial climate shifts controlled by ice sheet changes.
1321 *Nature*, 512 (7514), 290-294, doi:10.1038/nature13592, 2014.
- 1322 Zhisheng, A., Kutzbach, J.E., Prell, W.L., and Porter, S.C.: Evolution of Asian monsoons and phased uplift of the South

- 1323 Asian plateau since Late Miocene times. *Nature*, 411(6833), 62-66, 2001.
- 1324 Zhou, W. J., Lu, X. F., Wu, Z. K., Deng, L., Jull, A. J. T., Donahue, D. J., and Beck, W.: Peat record reflecting Holocene
1325 climate change in the Zoigê Plateau and AMS radiocarbon dating, *Chinese Sci. Bull.*, 47, 66-70,
1326 doi:10.1360/02tb9013, 2002.
- 1327

1328
1329
1330
1331
1332
1333
1334
1335
1336
1337
1338
1339
1340
1341
1342
1343
1344
1345
1346
1347
1348
1349
1350
1351
1352
1353
1354
1355
1356
1357
1358
1359
1360
1361
1362
1363
1364
1365
1366
1367
1368
1369
1370
1371
1372
1373
1374
1375
1376
1377
1378
1379
1380
1381
1382
1383
1384
1385
1386

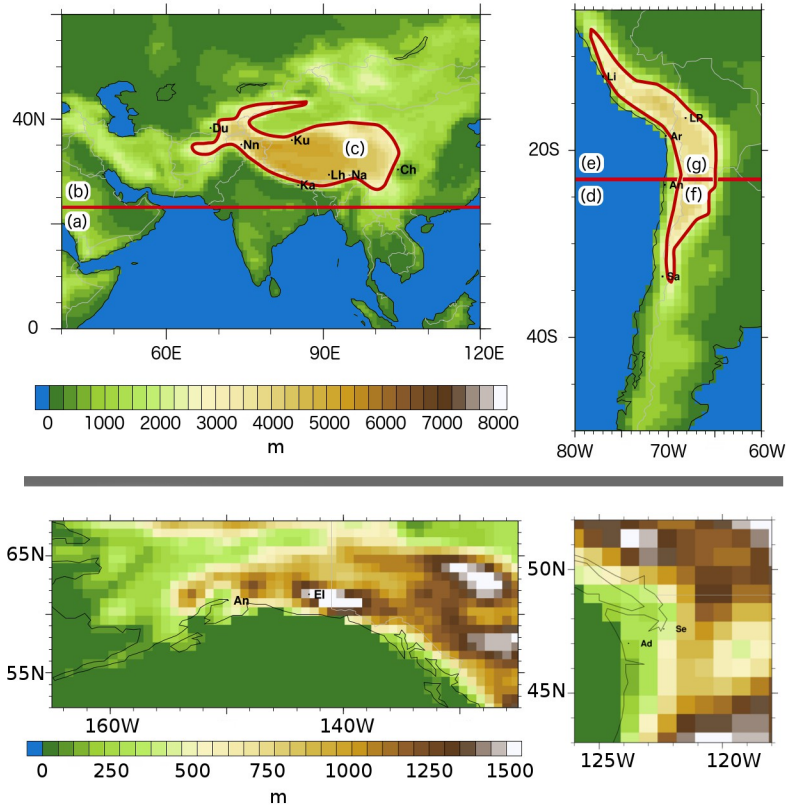


Figure 1

1387
 1388
 1389
 1390
 1391
 1392
 1393
 1394
 1395
 1396
 1397
 1398
 1399
 1400
 1401
 1402
 1403
 1404
 1405
 1406
 1407
 1408
 1409
 1410
 1411
 1412
 1413
 1414
 1415
 1416
 1417
 1418
 1419
 1420
 1421
 1422
 1423
 1424
 1425
 1426
 1427
 1428
 1429
 1430
 1431
 1432
 1433
 1434
 1435
 1436
 1437
 1438
 1439
 1440
 1441
 1442
 1443
 1444
 1445
 1446

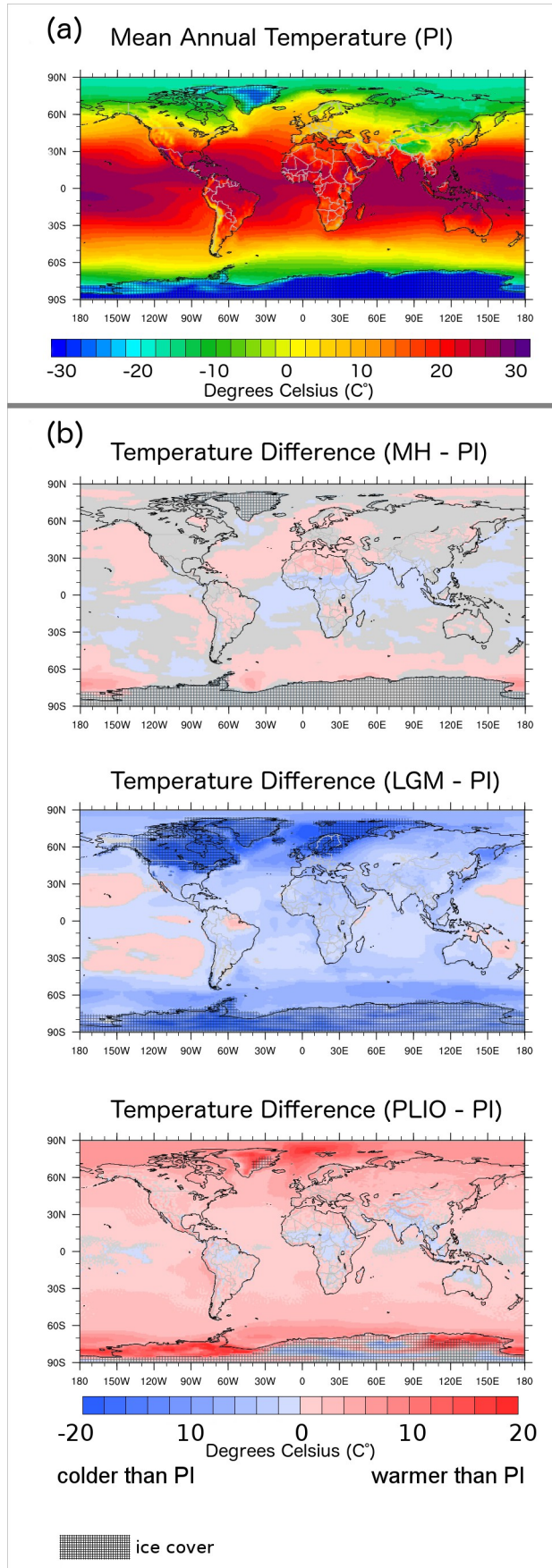


Figure 2

1447
1448
1449
1450
1451
1452
1453
1454
1455
1456
1457
1458
1459
1460
1461
1462
1463
1464
1465
1466
1467
1468
1469
1470
1471
1472
1473
1474
1475
1476
1477
1478
1479
1480
1481
1482
1483
1484
1485
1486
1487
1488
1489
1490
1491
1492
1493
1494
1495
1496
1497
1498
1499
1500
1501
1502
1503
1504
1505
1506

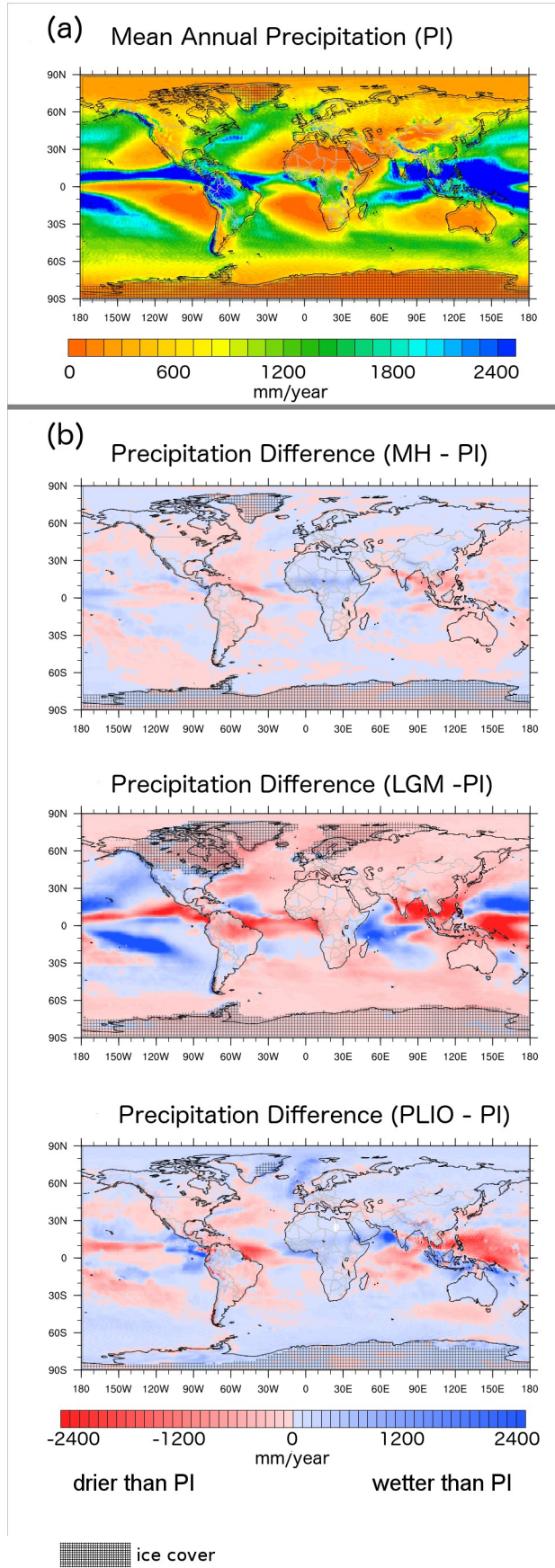


Figure 3

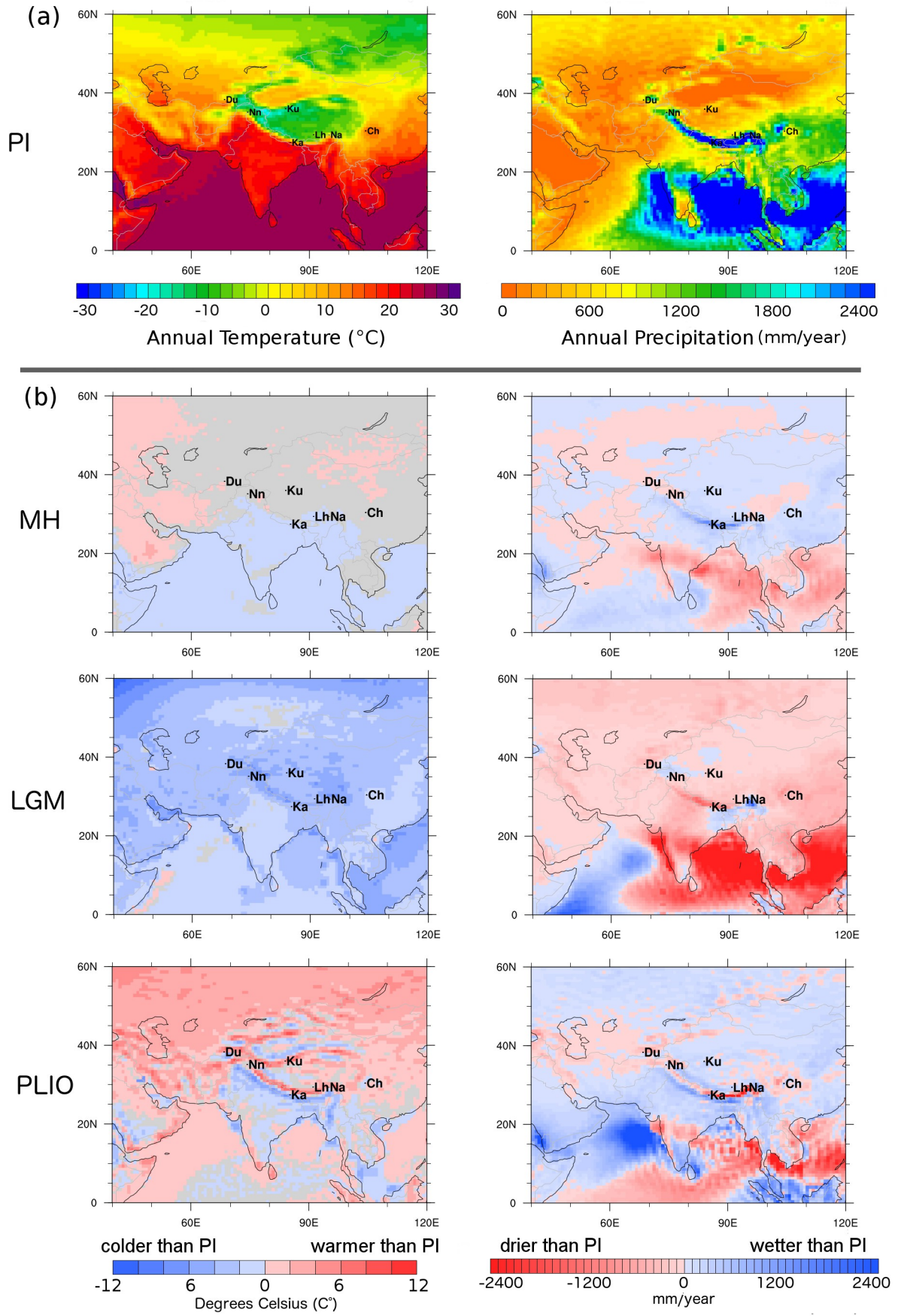


Figure 4

1510
1511
1512
1513
1514
1515
1516
1517
1518
1519
1520
1521
1522
1523
1524
1525
1526
1527
1528
1529
1530
1531
1532
1533
1534
1535
1536
1537
1538
1539
1540
1541
1542
1543
1544
1545
1546
1547
1548
1549
1550
1551
1552
1553
1554
1555
1556
1557
1558
1559
1560
1561
1562
1563
1564
1565
1566
1567
1568
1569

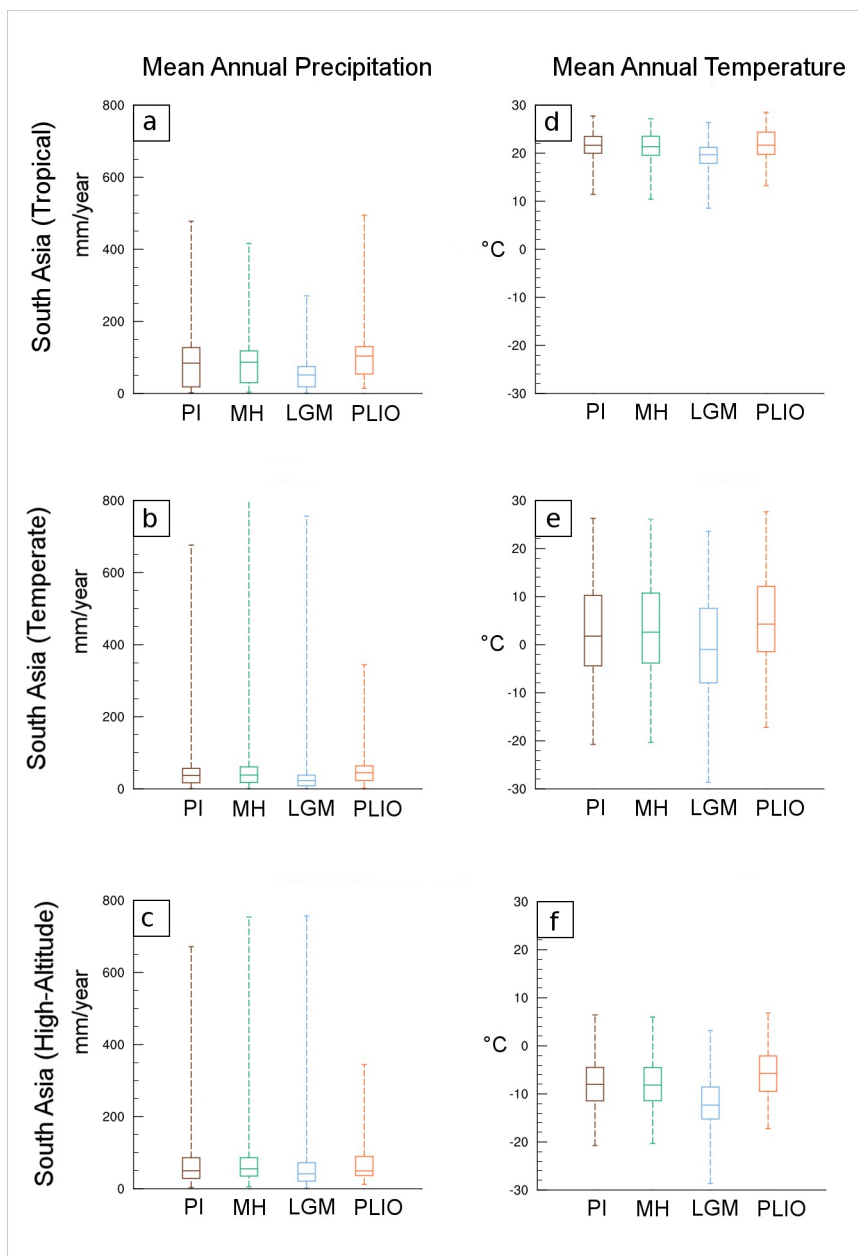
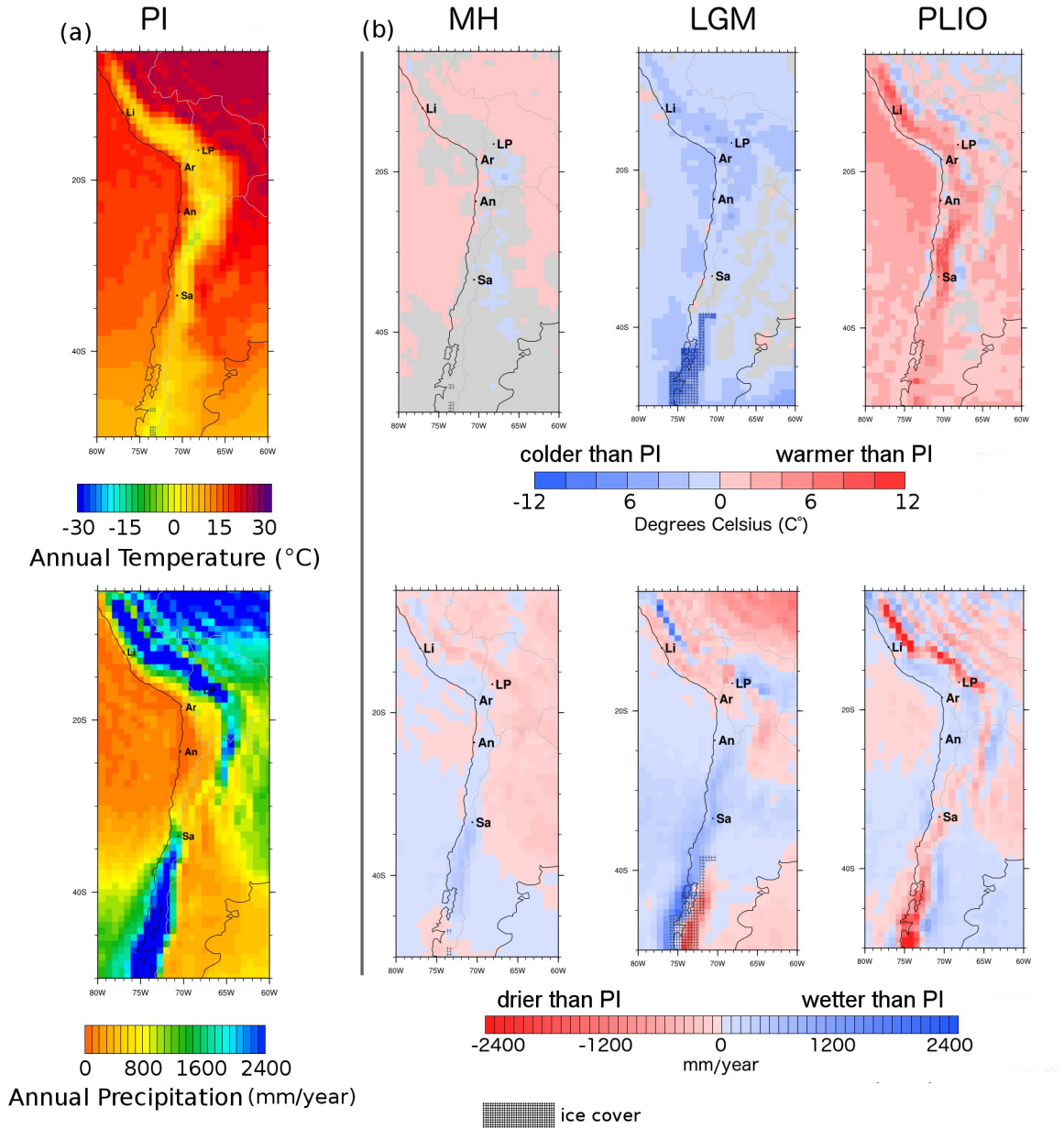


Figure 5

1630
 1631
 1632
 1633
 1634
 1635
 1636
 1637
 1638
 1639
 1640
 1641
 1642
 1643
 1644
 1645
 1646
 1647
 1648
 1649
 1650
 1651
 1652
 1653
 1654
 1655
 1656
 1657
 1658
 1659
 1660
 1661
 1662
 1663
 1664
 1665
 1666
 1667
 1668
 1669
 1670
 1671
 1672
 1673
 1674
 1675
 1676
 1677
 1678
 1679
 1680
 1681
 1682
 1683
 1684
 1685
 1686
 1687
 1688
 1689



1690
1691
1692
1693
1694
1695
1696
1697
1698
1699
1700
1701
1702
1703
1704
1705
1706
1707
1708
1709
1710
1711
1712
1713
1714
1715
1716
1717
1718
1719
1720
1721
1722
1723
1724
1725
1726
1727
1728
1729
1730
1731
1732
1733
1734
1735
1736
1737
1738
1739
1740
1741
1742
1743
1744
1745
1746
1747
1748
1749

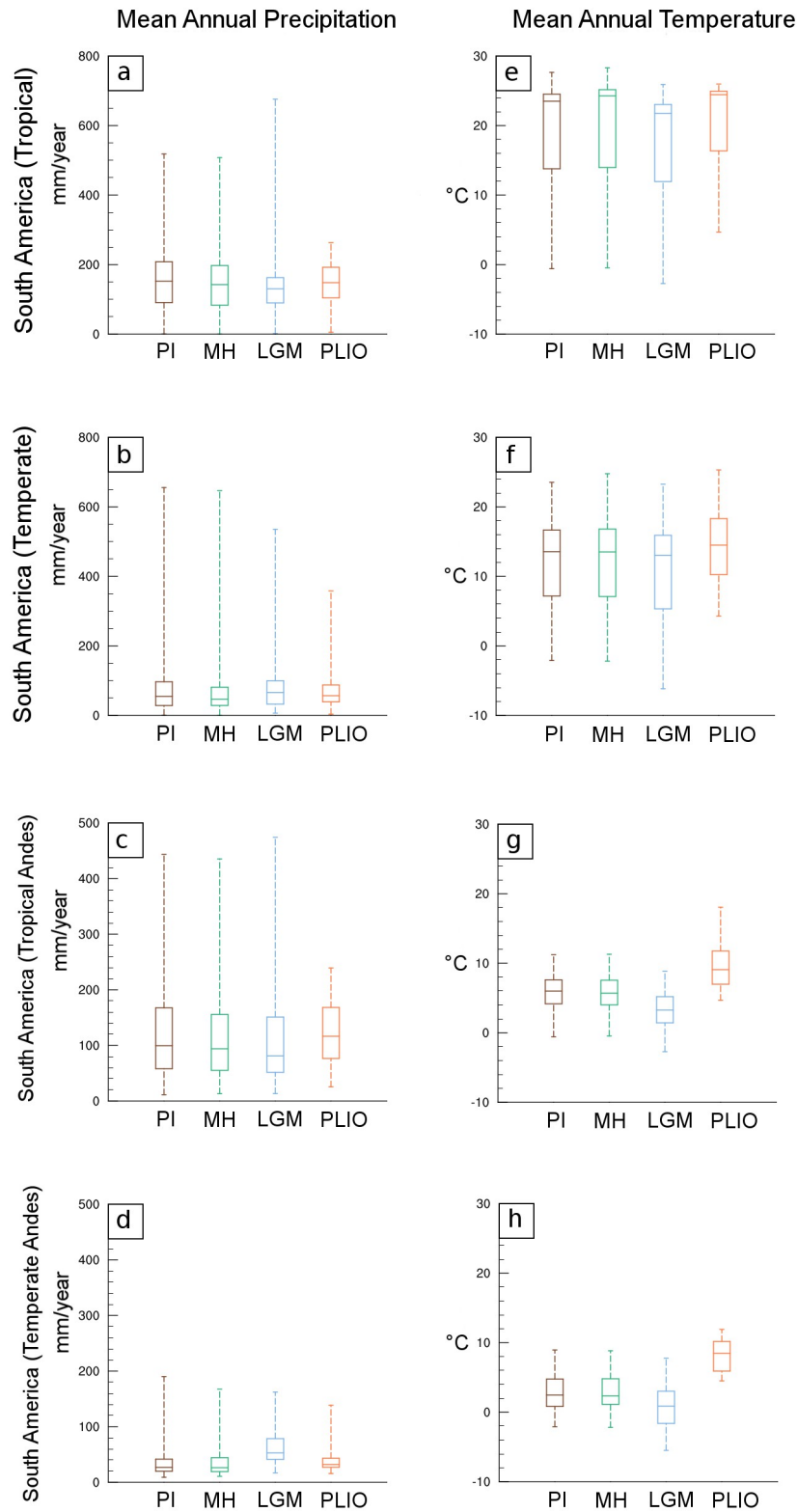


Figure 8

1750
1751
1752
1753
1754
1755
1756
1757
1758
1759
1760
1761
1762
1763
1764
1765
1766
1767
1768
1769
1770
1771
1772
1773
1774
1775
1776
1777
1778
1779
1780
1781
1782
1783
1784
1785
1786
1787
1788
1789
1790
1791
1792
1793
1794
1795
1796
1797
1798
1799
1800
1801
1802
1803
1804
1805
1806
1807
1808
1809

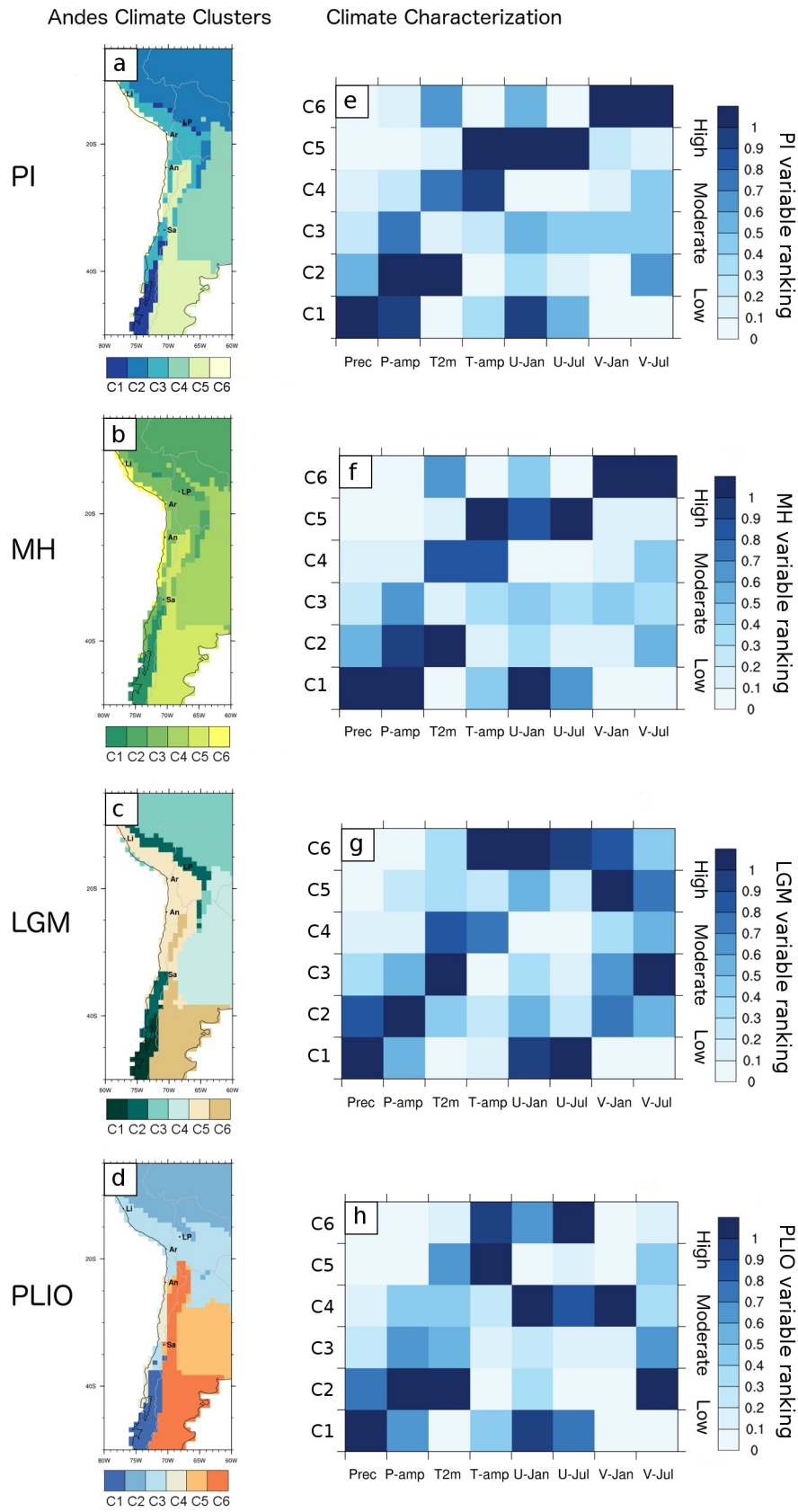


Figure 9

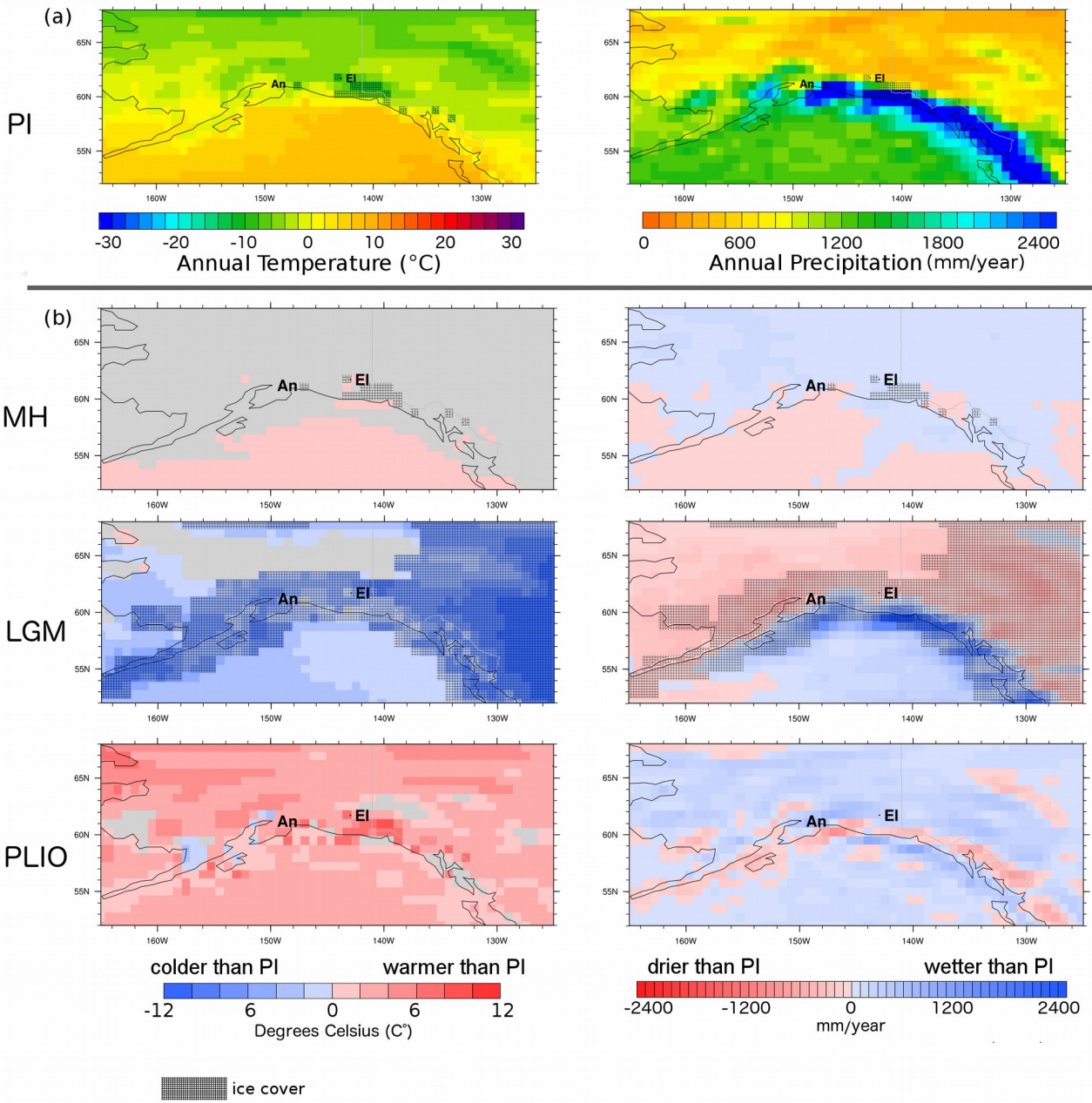


Figure 10

1811
1812
1813
1814
1815
1816
1817
1818
1819
1820
1821
1822
1823
1824
1825
1826
1827
1828

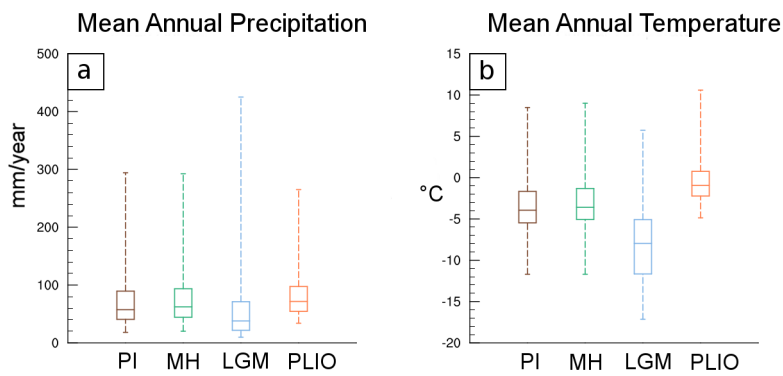


Figure 11

1829
 1830
 1831
 1832
 1833
 1834
 1835
 1836
 1837
 1838
 1839
 1840
 1841
 1842
 1843
 1844
 1845
 1846
 1847
 1848
 1849
 1850
 1851
 1852
 1853
 1854
 1855
 1856
 1857
 1858
 1859
 1860
 1861
 1862
 1863
 1864
 1865
 1866
 1867
 1868
 1869
 1870
 1871
 1872
 1873
 1874
 1875
 1876
 1877
 1878
 1879
 1880
 1881
 1882
 1883
 1884
 1885
 1886
 1887
 1888

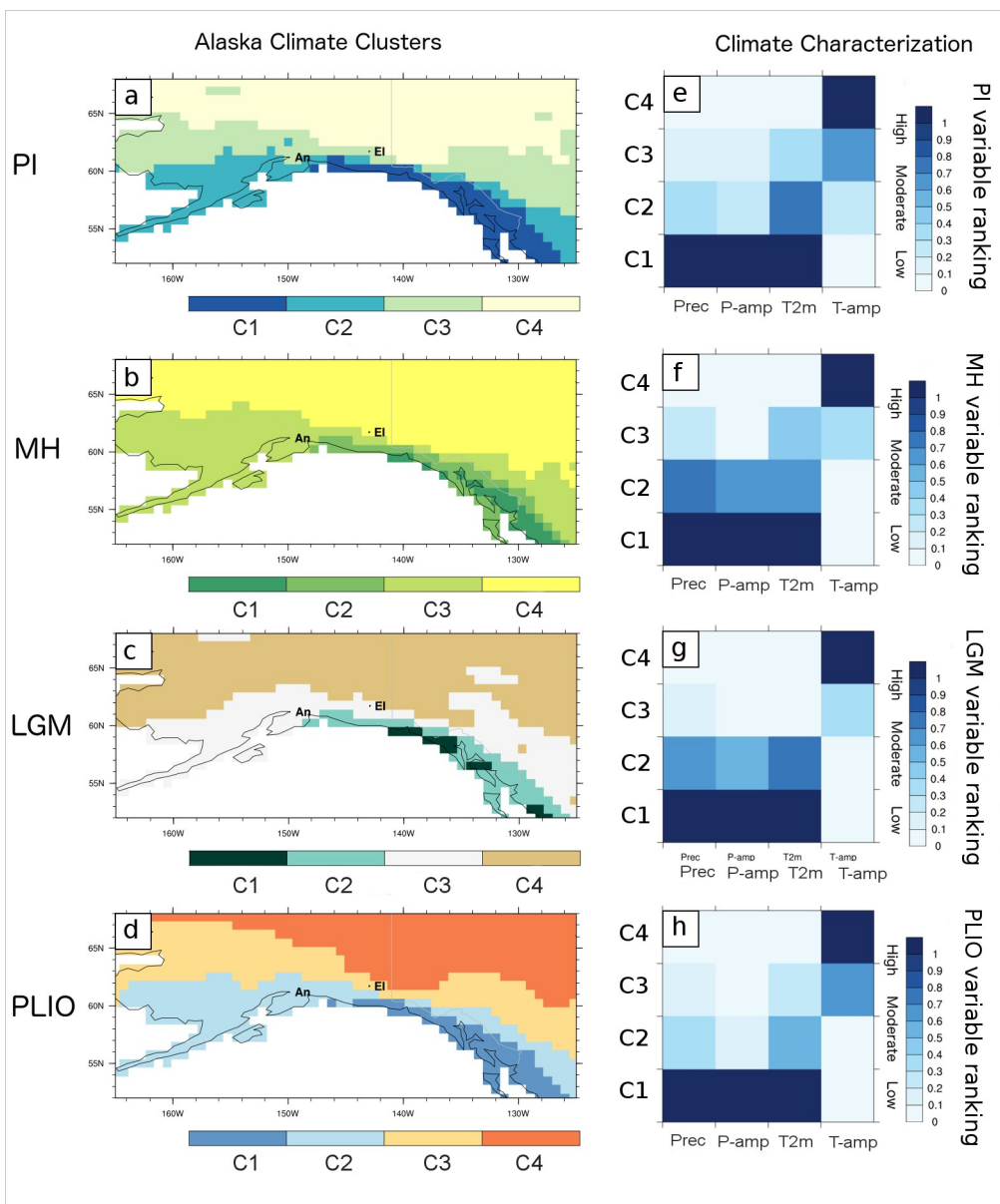


Figure 12

1889
1890
1891
1892
1893
1894
1895
1896
1897
1898
1899
1900
1901
1902
1903
1904
1905
1906
1907
1908
1909
1910
1911
1912
1913
1914
1915
1916
1917
1918
1919
1920
1921
1922
1923
1924
1925
1926
1927
1928
1929
1930
1931
1932
1933
1934
1935
1936
1937
1938
1939
1940
1941
1942
1943
1944
1945
1946
1947
1948

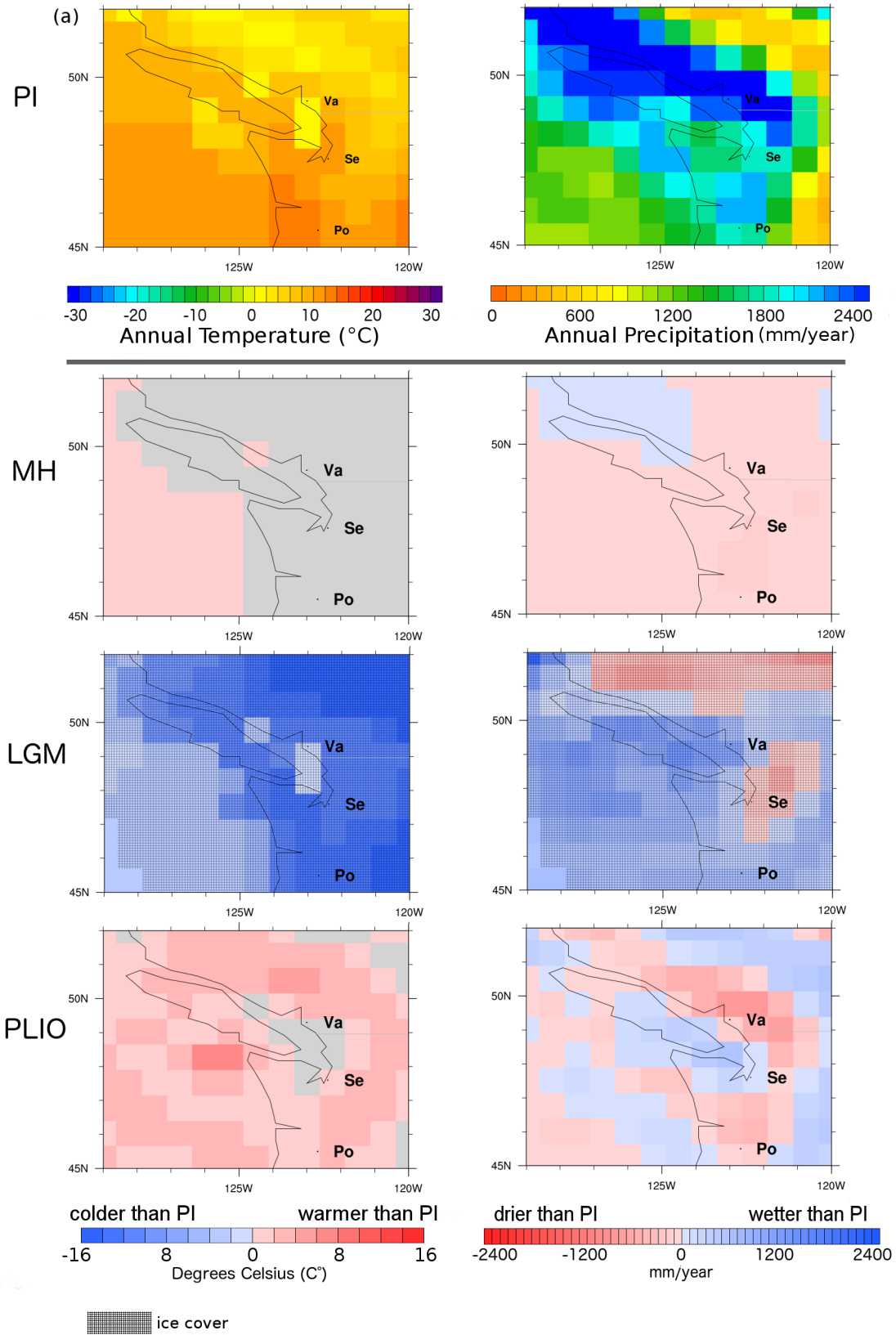


Figure 13

1949
1950
1951
1952
1953
1954
1955
1956
1957
1958
1959
1960
1961
1962
1963
1964
1965
1966
1967
1968
1969
1970
1971
1972
1973
1974
1975
1976
1977
1978
1979
1980
1981
1982
1983
1984
1985
1986
1987
1988
1989
1990
1991
1992
1993
1994
1995
1996
1997
1998
1999
2000
2001
2002
2003
2004
2005
2006
2007
2008

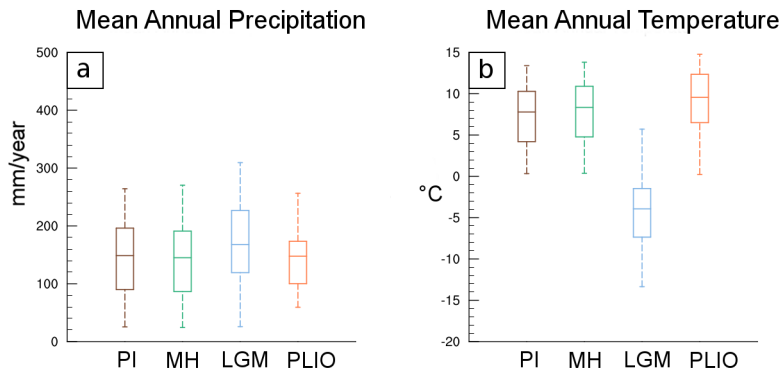


Figure 14

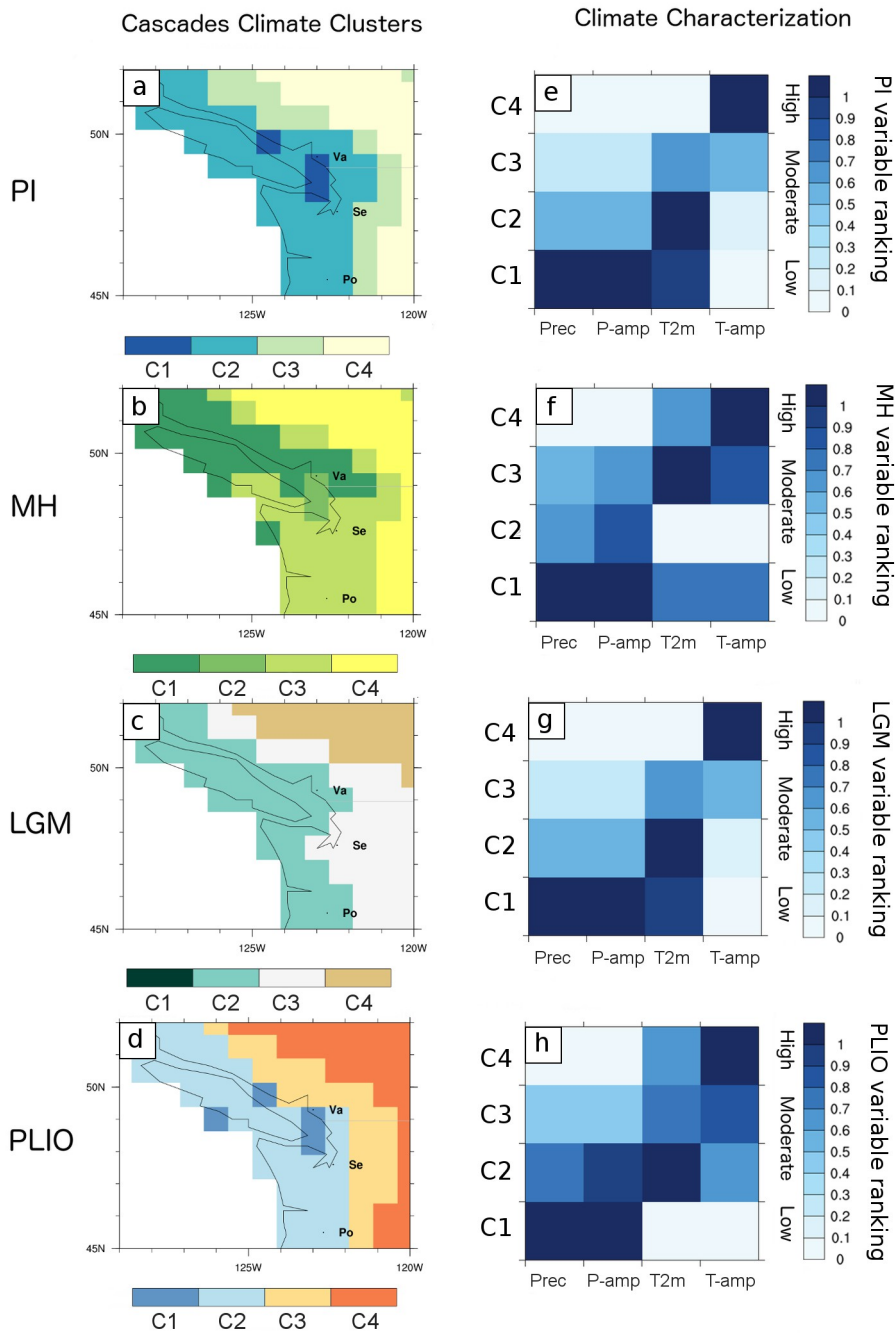


Figure 15

2009
2010
2011
2012
2013
2014
2015
2016

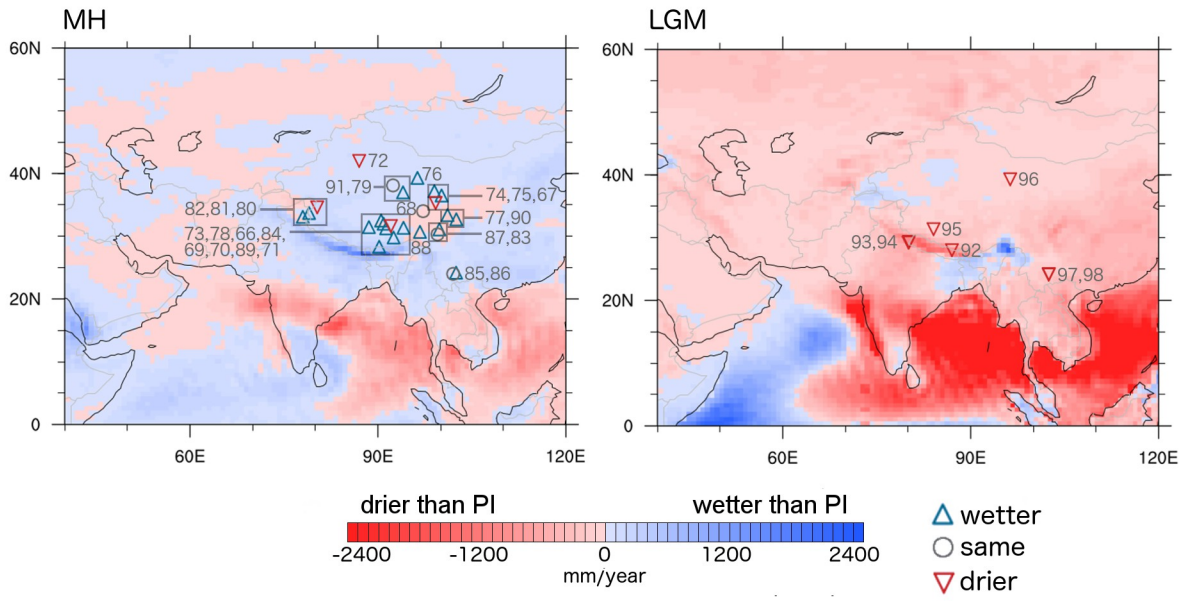


Figure 16

2017
2018
2019
2020
2021
2022
2023
2024
2025
2026
2027
2028
2029
2030
2031
2032
2033
2034
2035
2036
2037
2038
2039
2040
2041
2042
2043
2044
2045
2046
2047
2048
2049

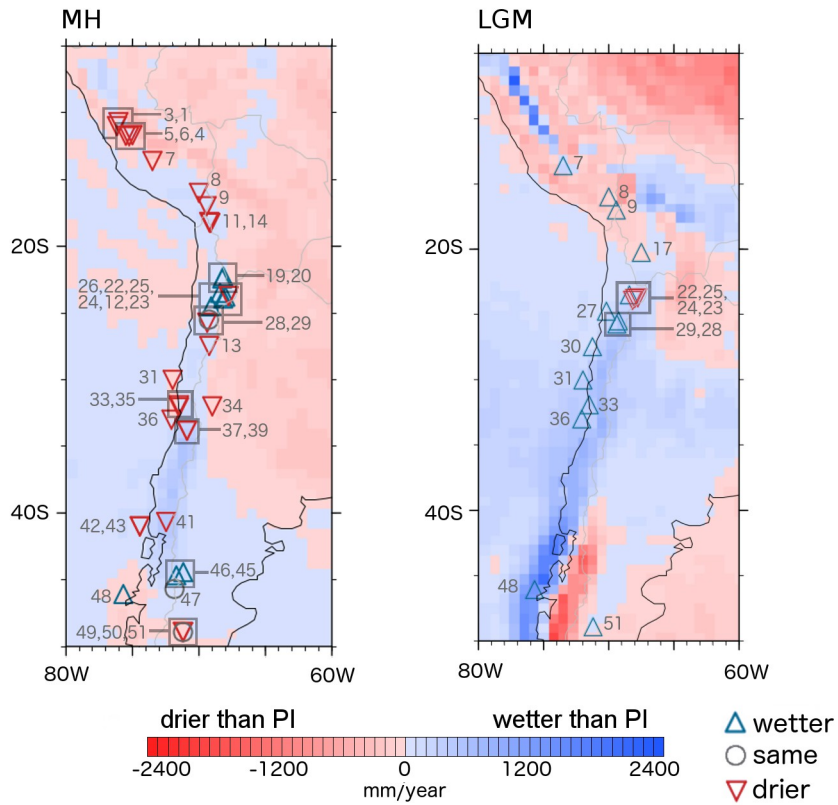


Figure 17